Journal of Sound and Vibration (2001) **244**(2), 259–297
doi:10.1006/jsvi.2000.3456, available online at http://www.idealibrary.com on IDEAL®

A MODAL EXPANSION ANALYSIS OF NOISE TRANSMISSION THROUGH CIRCULAR CYLINDRICAL SHELL STRUCTURES WITH BLOCKING MASSES

P. Gardonio, N. S. Ferguson and F. J. Fahy

Institute of Sound and Vibration Research, University of Southampton, Southampton SO17 1BJ, England. E-mail pg@isvr.soton.ac.uk

(*Received* 13 *January* 2000, *and in final form* 11 *October* 2000)

This paper covers the development and application of a modal interaction analysis (MIA) to investigate the plane wave transmission characteristics of a circular cylindrical sandwich shell of the type used in the aerospace industry for satellite launch vehicles. The model is capable of handling many high order structural and acoustic modes, and can be used to investigate the sensitivity to different structural stiffness configurations, angles of incidence, damping and cavity absorption. The model has been developed to predict the structural response and transmitted noise when a number of discrete masses are applied to the shell. The study presented considers a set of cases where blocking masses, having a total weight equal to 8% of the cylinder weight, are attached to the cylinder. The simulations carried out show a substantial reduction of the sound transmission in many of the first 15 one-third octave frequency bands (frequency range 22·4–707 Hz). The blocking masses act on the shape of the cylinder normal modes and their orientations with respect to the plane of the incident wavenumber vector. In particular, the circumferential re-orientation reduces the coupling between the incident acoustic field and the structural modes of the cylinder. The modification of the structural mode shapes, both in axial and circumferential directions, also reduces the coupling between the cylinder modes and the acoustic modes of the interior.

Simulations show the effect of the number of structural and acoustic modes included on the calculated frequency response, and indicate the number necessary for an accurate prediction of the resonant and non-resonant sound transmission through the structure. In particular, the effect of neglecting off-resonance acoustic and structural modes is investigated. It is shown that restricting the acoustic and structural modes to those having natural frequencies within an interval of ± 40 and ± 60 Hz, respectively, of the excitation frequency produces acceptably small errors in the transmission estimate. The simulations also show that in order to represent accurately the coupling effect between the structural and acoustic modes, for each acoustic mode of order m_a, n_a, p_a (axial, circumferential and radial order, respectively), it is necessary to account only for the structural modes with $n_s = n_a$ and $m_s = m_a \pm \alpha$ with $\alpha = 1, 3, 5, \ldots, \alpha_{max}$. It is found that the time required to compute the sound transmission in a frequency range of 0–3123 Hz, using the minimum number of acoustic and structural modes required to compute an accurate response at each frequency, is 3% of that necessary for the computation of the full response using all the structural and acoustic modes with natural frequencies within the frequency range considered in the analysis.

1. INTRODUCTION

The assessment of the relative contribution to the transmission of sound by resonant and non-resonant cylindrical shell vibration is an important and complex problem. Various

0022-460X/01/270259 + 39 $35.00/0

models have been developed to analyze and predict the acoustic behaviour of aircraft fuselages, the effect of resonances, and the divergence from mass-law transmission [1]. In many applications, the external acoustic field is assumed either to be diffuse, or is plane and incident upon the structure at a specified angle and direction. The structure, if stiffened, may be analyzed using a Rayleigh–Ritz formulation for its modal characteristics [2]. Koval [3] investigated the transmission loss (TL) of an infinitely long isotropic thin cylindrical shell as a function of curvature, flow and pressurization effects. He observed total scattering and zero transmission as a function of flow speed and internal and external speed of sound. The transmission loss exhibited minima at the ring frequency and at the critical frequency of the structure. Below the ring frequency, the cylinder resonances were found to affect the transmission loss, and between the ring frequency and critical frequency the shell was found to follow mass-law behaviour. Barbe *et al.* [4] used the analytical and numerical model developed by Koval to investigate the effect of the zeros of the circular cylinder impedance and explained why a change of slope and dips are observed in the transmission loss curves at about the ring frequency. Blaise *et al.* [5] compared the transmission losses caused by diffuse field excitation and normally incident plane wave excitation. Koval [6] also analyzed the transmission loss of an infinitely long orthotropic thin cylindrical shell. Blaise *et al.* [7] extended Koval's studies to the case of plane acoustic waves with two independent angles of incidence in order to calculate the diffuse field transmission coefficient. Blaise and Lesueur [8–10] have derived expressions for the acoustic transmission through 2-D and 3-D orthotropic multi-layered infinite cylindrical shells.

Statistical models and techniques have also been used to estimate the sound power transmitted into cavities [11]. Where only few modes of the structure and the cavity are resonant in a frequency range of interest, the energy flow between the individual structural modes and the acoustic modes of the cavity is analyzed using the assumption of weak coupling. In this case the sound transmission is analyzed using the assumption that the natural frequencies and mode shapes of the structural modes are similar to the *in vacuo* modes. The analysis allows for well-coupled modes in terms of closely spaced resonance frequencies of the structural and acoustic modes and calculates band-averaged power into the internal acoustic space. Reference [11] forms the basis of the analysis for the present study, but the restriction of averaging the results over frequency bands is removed and allows the effect of the sensitivity to frequency matching to be considered. Further development of this form of analysis by Pope and Wilby [12] considered the transmission of sound into non-resonant acoustic modes within a frequency band by evaluating the band-averaged response of these modes in addition to that of the resonant acoustic modes.

Structural modification is one approach to changing the transmission loss. The effect of increased damping [13] is to reduce the resonant structural response; this is observed to raise the minima in the transmission loss at the resonances and also at the ring and coincidence frequencies. Some benefit in the mass-law controlled region is also observed. Longitudinal stiffeners [14] appear to increase the cylinder transmission loss in the mass-controlled region but with a consequence of dips at the stringer resonances. Dowell [15] considered a double-wall cylindrical structure subject to the acoustic field, generated by a propeller, which was expressed as a summation of circumferential waves. Benefits are achieved if the inner shell is stiffer than the outer, so that it has smaller displacements, and if the natural frequencies of the shells are separated (detuned). If the shells are fairly similar in properties then they can be well coupled through the intervening fluid which can result in greater transmission of noise. Aerospace structures of composite and sandwich construction can be similarly analyzed in terms of the structural modes [16, 17], although the results presented in reference [17] are for a composite with a soft viscoelastic core which introduces

significant structural damping. The present study concentrates on the analysis of cylindrical sandwich shells with a stiff core, as used for spacecraft launcher construction, and the possibility of noise control by mass changes.

Analytical models based on a modal expansion of the structural and acoustic fields have been developed and applied to the investigation of noise in a propeller driven aircraft [18–20]. Three different models of sound transmission through the fuselage of an aircraft are available, depending on the frequency range of the problem being considered [21]. At low frequencies, when the longitudinal and circumferential wavelength of the fuselage skin flexural vibrations are longer than the stiffeners spacing (ring frames and stringers), the sound transmission into the cabin may be calculated using a "smeared" shell model. This type of model represents the sound transmission through the fuselage considered as an equivalent orthotropic cylindrical skin whose dynamics incorporate the mass and stiffness effects of the stiffeners. Alternatively, one can analyze a monocoque shell with rings and stiffeners treated as discrete structural elements. For higher frequencies, in the low-intermediate frequency range, the vibrations of the frames become less important so that only the effects of the fuselage skin and longitudinal stringers need to be considered in the calculation of the noise transmission of a fuselage section between two adjacent frames. For relatively high frequencies the dynamics of the stringers no longer strongly affect the fuselage skin vibration. In order to calculate the noise transmission it is then necessary to consider only a section of the fuselage skin confined between two adjacent frames and two adjacent stringers. A statistical energy approach is then appropriate as the number of modal contributions is high and individual modal couplings cannot be individually formulated. Instead, the averaged coupling and response is calculated in frequency bands [1].

The study presented here considers the acoustic response of a honeycomb cylindrical shell, filled with air, which is externally excited by a plane acoustic wave. In particular, the effects of blocking masses placed on the surface of the cylinder is investigated in order to assess the possibility of reducing the external coupling (acoustic plane wave excitation—cylinder response) and internal coupling (cylinder vibration—cavity response) of the system. The goal is to reduce the sound transmission to the interior of the cylinder. For the purposes of this study a model has been developed which is valid in the low-intermediate frequency range and allows the steady state acoustic response of the cavity to be calculated at discrete frequencies for harmonic external plane waves of unit amplitude. In this way, the noise reduction for one-third octave bands has been evaluated.

The noise reduction evaluated for the reference case of the cylinder without masses is compared with the noise reduction of a set of cases where the cylinder is modified by the addition of a set of blocking masses. The dimensions of the cylinder and the geometrical and physical properties of the honeycomb wall have been selected with reference to a scale model of the payload section of the ARIANE 5 launcher. The effects produced by the blocking masses, on both the external and internal coupling, are then analyzed in detail by considering the mode shapes of the cylinder with masses.

The effect of the number of acoustic modes ("*acoustic flagging*"), or structural modes ("*structural flagging*" and "*coupling flagging*"), selected to compute the response at each discrete frequency is also assessed. A reduction of the number of acoustic and structural modes taken into account in the modal formulation gives considerable advantages in terms of computational speed. Cacciolati *et al.* [22] first considered the possibility of reducing the computational time required to calculate the sound transmission to the interior of a cylinder with the modal method. They proposed to select the structural and acoustic modes with strongest coupling either in the frequency or spatial domains.

2. MATHEMATICAL MODEL AND ANALYSIS

The method used in this study is modal interaction analysis (MIA) [23]. It is based upon a circumferential and axial decomposition of the external noise field, a modal description of the fairing modelled as a honeycomb sandwich cylindrical shell, and a modal description of the interior acoustic cavity. Dissipation and radiation damping of the shell are included and, in addition, one can represent the case when the internal volume is partly filled by a payload. This form of analysis is more appropriate than statistical energy analysis (SEA), since the restriction to diffuse external acoustic fields is not necessary, and the frequency region of most concern, where there is low modal overlap, can be investigated in detail. In addition, development of the method can allow for mass non-uniformity, which thereby perturbs the natural frequencies of the structure and also causes the structural modes to be modified, thereby altering the coupling to the external sound field.

The main assumption of the analysis is that the coupling between the interior acoustic cavity modes and the shell structural modes is weak. The fully coupled equations of motion of the acoustic and structural modes are replaced by simplified uncoupled equations that express the response of the *in vacuo* structural modes and the response of the acoustic cavity modes to excitation by the structural motion [15, 24]. This approximation yields maxima in the response near the uncoupled mode resonance frequencies instead of at frequencies corresponding to the resonance frequencies of the coupled system, although the assumption is reasonable when the internal acoustic resonances are well damped [15].

Due to the simple cylindrical geometry, the modes of the uniform shell and interior cavity have sinusoidal/cosinusoidal circumferential variation of integer orders n_s and these modes are orthogonal for mode pairs of different order. Simple spatial selection occurs such that structural modes of circumferential order n_s will only contribute to the internal acoustic field of the same circumferential order $n_a = n_s$. This selectivity is not available when the shell becomes non-uniform as each mode of the shell can possess a circumferential variation composed of a number of different circumferential orders, as in a Fourier expansion.

The MIA formulation can be further simplified by selecting at each frequency a subset of the modes with natural frequencies within the frequency range considered in the analysis. For example the noise transmission at each frequency can be calculated by taking into account only the structural and/or acoustic modes with natural frequencies close to the frequency considered, although this is not necessarily accurate.

Figure 1 shows the idealized model excited by an external incident acoustic plane wave having a wavenumber vector at an angle ϕ_i to the cylinder axis and θ_i in the azimuthal direction. The blocked pressure field is calculated on the cylinder surface using a diffraction model. The incident field is decomposed into a series of cylindrical components relative to each circumferential structural mode of order n_s. Each of these components is a function of frequency termed the "scattering coefficient" for circumferential order n_s. The generalized forces acting on the uncoupled, *in vacuo* structural modes of the cylinder are then evaluated. The response of the shell, in terms of these structural modes, is calculated and then the response of the interior acoustic cavity, in terms of the uncoupled acoustic modes, is calculated from the shell motion acting at the boundary of the acoustic volume.

The analysis, based on references [23, 24], expresses the shell response and interior acoustic cavity response in terms of the *in vacuo* structural modes $\Psi_n = \Psi_{m_s n_s}$ and uncoupled interior cavity modes $\Phi_p = \Phi_{m_a n_a p_a}$, for the fluid in the cavity with rigid boundaries. The shell response is represented by the summation $\sum_n w_n \Psi_n$, while the interior pressure is represented by $\sum_p p_p \Phi_p$ where w_n and p_p are the modal displacement and pressure generalized co-ordinates respectively. Substituting the modal terms into the *in vacuo*

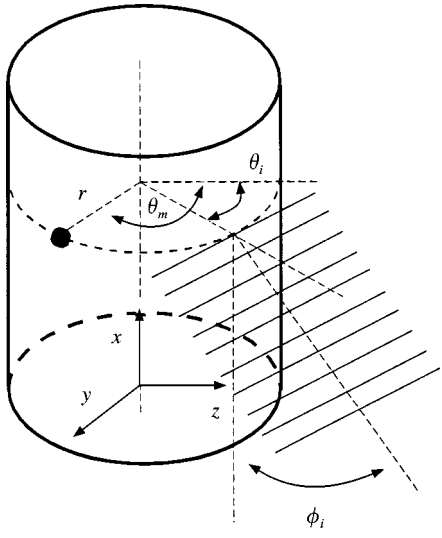

Figure 1. Co-ordinate system of the model.

equations of motion of the structure and the fluid, multiplying by the corresponding mode shapes and applying orthogonality of the modes, the following modal equations for the structure and the fluid are obtained [23, 24]:

$$\ddot{w}_n + \omega_n^2 w_n = \frac{S}{\Lambda_n} \sum_p p_p C_{np} + \frac{F_n}{\Lambda_n}, \tag{1}$$

$$\ddot{p}_p + \omega_p^2 p_p = \left(\frac{\rho c^2 S}{\Lambda_p}\right) \sum_n \ddot{w}_n C_{np} + \frac{\rho c^2 \dot{Q}_p}{\Lambda_p}, \tag{2}$$

where F_n is the generalized force acting on the cylinder surface, ω_n is the natural frequency of a cylinder mode, C_{np} is a dimensionless coupling coefficient, S is the cylinder surface area, Λ_n is the normalization (generalized mass) for the modes of the cylinder, ω_p is the natural frequency of an acoustic mode, ρ is the mean density of the fluid, c is the speed of sound in the fluid, Λ_p is the normalization (generalized mass) for the modes of the acoustic cavity and $\dot{Q}_p$ is the generalized acoustic source strength, if any, in the cavity.

The details on the calculation of the natural frequencies and mode shapes, of the structure and the internal fluid, and the derivation of the forcing terms and coupling terms are presented in the following sections. Where the structure is non-uniform, the mode shapes are themselves given by a series summation and each term in the series can be coupled to the appropriate external and internal acoustic fields by equations (1) and (2) above.

2.1. CALCULATION OF THE NATURAL FREQUENCIES AND NATURAL MODES OF A UNIFORM HONEYCOMB CYLINDER

The simplest cylindrical sandwich shell, supported on shear diaphragm ends, has modes that can be described by three components of displacement (radial, axial and tangential) and two rotations. The external acoustic field excites the cylinder in bending. Bending wave motion is characterized by both radial displacement, $w(r, \theta, t)$, and angular displacements,

$\theta_x(r, \theta, t)$ and $\theta_y(r, \theta, t)$. However, the coupling between the cylinder and the fluid in the cavity is determined only by the radial vibration of the cylinder. Thus, only the radial motion of the cylinder is considered. The radial displacement of the cylinder has circumferential variation given by $\sin n_s\theta$ and $\cos n_s\theta$, to allow for unspecified orientation, and variation $\sin(m_s\pi x/L)$ in the axial direction. Substituting for the functions of the five components of displacement into the boundary conditions at the ends of a cylinder of length L produces five equations for modes of order (m_s, n_s) that satisfy the following matrix equations which can be assembled in an eigenvalue form:

$$\mathbf{A}\mathbf{x}_j = \mathbf{\Lambda}_j\mathbf{B}\mathbf{x}_j, \tag{3}$$

where

$$\mathbf{\Lambda}_j = \begin{bmatrix} \lambda_{uj} & & & & \\ & \lambda_{vj} & & 0 & \\ & & \lambda_{wj} & & \\ & 0 & & \lambda_{\theta xj} & \\ & & & & \lambda_{\theta yj} \end{bmatrix}, \quad \mathbf{x}_j = \begin{Bmatrix} x_{uj} \\ x_{vj} \\ x_{wj} \\ x_{\theta xj} \\ x_{\theta yj} \end{Bmatrix}. \tag{4}$$

$\lambda_{uj} = \omega_{uj}^2$, $\lambda_{vj} = \omega_{vj}^2$, $\lambda_{wj} = \omega_{wj}^2$, $\lambda_{\theta xj} = \omega_{\theta xj}^2$ and $\lambda_{\theta yj} = \omega_{\theta yj}^2$ are the jth natural frequencies squared, equal to the eigenvalues, and x_{uj}, x_{vj}, x_{wj}, $x_{\theta xj}$ and $x_{\theta yj}$ are the jth natural mode amplitudes, respectively, for the x, y, z, θ_x and θ_y degrees of freedom, equivalent to the eigenvectors of the problem. Matrices **A** and **B** are given in reference [25]. The five modes found for each particular (m_s, n_s) pair correspond to modes that possess displacements with both radial displacement, and in-plane displacement and also rotations. There is a selection of the modes that are primarily radial as the other modes are either not excited or are at much higher frequencies and are not of interest with insignificant radial components. The selected modes are subsequently used in a series expansion in the following section.

2.2. CALCULATION OF THE NATURAL FREQUENCIES AND NORMAL MODES OF A HONEYCOMB CYLINDER WITH ATTACHED POINT MASSES

The modes of the uniform sandwich cylinder are used in a Rayleigh–Ritz analysis to include the effect of an additional number of discrete point masses. The potential energy of the system is assumed to be unaltered by the mass, with changes only to the kinetic energy of the system.

The displacement of the non-uniform shell is expressed in an approximate series form as

$$\begin{Bmatrix} u(t) \\ v(t) \\ w(t) \end{Bmatrix} = \sum_{m_s=1}^{M_s} \sum_{n_s=0}^{N_s} p_{m_sn_s}(t) \begin{Bmatrix} A_{m_sn_s} \cos n_s\theta \cos \dfrac{m_s\pi x}{\ell} \\ B_{m_sn_s} \sin n_s\theta \sin \dfrac{m_s\pi x}{\ell} \\ C_{m_sn_s} \cos n_s\theta \sin \dfrac{m_s\pi x}{\ell} \end{Bmatrix} + q_{m_sn_s}(t) \begin{Bmatrix} A_{m_sn_s} \sin n_s\theta \cos \dfrac{m_s\pi x}{\ell} \\ B_{m_sn_s} \cos n_s\theta \sin \dfrac{m_s\pi x}{\ell} \\ C_{m_sn_s} \sin n_s\theta \sin \dfrac{m_s\pi x}{\ell} \end{Bmatrix}, \tag{5}$$

where m_s and n_s represent the structural modes with n_s circumferential wavelengths and m_s half-axial wavelengths, $p_{m_sn_s}$, $q_{m_sn_s}$ are the generalized co-ordinates of the even and odd modes in θ, $A_{m_sn_s}$ $B_{m_sn_s}$ and $C_{m_sn_s}$ are the relative contributions of the u, v and w displacements in the "new" structural mode; finally u, v, w are the in-plane (axial), tangential and flexural

(normal to circumference) components of the mode. It is a necessary requirement to include both even and odd functions in θ to allow the "new" modes of the non-uniform shell to be orientated circumferentially due to the non-uniform mass distribution.

The modes of the uniform shell are orthogonal which implies that the kinetic and strain energy can be expressed in terms of diagonal mass and stiffness matrices as follows:

$$T_{cyl} = \frac{1}{2}[\dot{\mathbf{p}}^{\mathrm{T}} \;\; \dot{\mathbf{q}}^{\mathrm{T}}] \cdot [\mathbf{M}] \cdot \begin{bmatrix} \dot{\mathbf{p}} \\ \dot{\mathbf{q}} \end{bmatrix} \tag{6}$$

and

$$U_{cyl} = \frac{1}{2}[\mathbf{p}^{\mathrm{T}} \;\; \mathbf{q}^{\mathrm{T}}] \cdot [\mathbf{K}] \cdot \begin{bmatrix} \dot{\mathbf{p}} \\ \dot{\mathbf{q}} \end{bmatrix}, \tag{7}$$

where $\mathbf{p}^{\mathrm{T}} = \{p_{10}, p_{11}, \ldots, p_{1N_s}, p_{20}, \ldots, p_{M_sN_s}\}$ and $\mathbf{q}^{\mathrm{T}} = \{q_{10}, q_{11}, \ldots, q_{1N_s}, q_{20}, \ldots, q_{M_sN_s}\}$. The attached discrete point masses contribute only to the kinetic energy. For a mass m_k attached at $x = x_i$ and angle $\theta = \theta_k$, with respect to incidence of external acoustic field (i.e., $\theta_k = \theta_m - \theta_i$ as shown in Figure 1), the associated kinetic energy is given by the following relation, assuming negligible rotational inertia:

$$T_{m_k} = \frac{1}{2} m_k \left\{ \sum_{m_s=1}^{M_s} \sum_{n_s=0}^{N_s} \dot{p}_{m_sn_s}(t) \begin{Bmatrix} A_{m_sn_s} \cos n_s\theta_k \cos \dfrac{m_s\pi x_i}{\ell} \\ B_{m_sn_s} \sin n_s\theta_k \sin \dfrac{m_s\pi x_i}{\ell} \\ C_{m_sn_s} \cos n_s\theta_k \sin \dfrac{m_s\pi x_i}{\ell} \end{Bmatrix} + \dot{q}_{m_sn_s}(t) \begin{Bmatrix} A_{m_sn_s} \sin n_s\theta_k \cos \dfrac{m_s\pi x_i}{\ell} \\ B_{m_sn_s} \cos n_s\theta_k \sin \dfrac{m_s\pi x_i}{\ell} \\ C_{m_sn_s} \sin n_s\theta_k \sin \dfrac{m_s\pi x_i}{\ell} \end{Bmatrix} \right\}^2, \tag{8}$$

which, similar to equation (6), can be expressed as follows:

$$T_{m_k} = \frac{1}{2}[\dot{\mathbf{p}}^{\mathrm{T}} \;\; \dot{\mathbf{q}}^{\mathrm{T}}] \cdot [\mathbf{M}_k] \cdot \begin{bmatrix} \dot{\mathbf{p}} \\ \dot{\mathbf{q}} \end{bmatrix}, \tag{9}$$

where the rows of the matrix $[\mathbf{M}_k]$ are obtained by considering the coefficients relative to the parameters $p_{10}, p_{11}, \ldots, p_{1N_s}, p_{20}, \ldots, p_{M_sN_s}$ and $q_{10}, q_{11}, \ldots, q_{1N_s}, q_{20}, \ldots, q_{M_sN_s}$ in the expressions derived by differentiating the total kinetic energy of the masses with reference to time and to the parameters $p_{10}, p_{11}, \ldots, p_{1N_s}, p_{20}, \ldots, p_{M_sN_s}$ and $q_{10}, q_{11}, \ldots, q_{1N_s}, q_{20}, \ldots, q_{M_sN_s}$:

$$\begin{matrix} \dfrac{\mathrm{d}}{\mathrm{d}t}\left(\dfrac{\partial T_{m_k}}{\partial \dot{p}_{10}}\right) \\ \vdots \\ \dfrac{\mathrm{d}}{\mathrm{d}t}(\partial T_{m_k}/\partial \dot{p}_{M_sN_s}) \\ \dfrac{\mathrm{d}}{\mathrm{d}t}(\partial T_{m_k}/\partial \dot{q}_{10}) \\ \vdots \\ \dfrac{\mathrm{d}}{\mathrm{d}t}\left(\dfrac{\partial T_{m_k}}{\partial \dot{q}_{M_sN_s}}\right) \end{matrix} \Rightarrow [\mathbf{M}_k]. \tag{10}$$

For example, the elements of the first row of the matrix $[\mathbf{M}_k]$ are calculated as follows:

$$\frac{\mathrm{d}}{\mathrm{d}t}\left(\frac{\partial T_{m_k}}{\partial \dot{p}_{10}}\right) = -\omega^2\{M_{1,1}p_{10} + \cdots + M_{1,N_s+1}p_{1N_s} + M_{1,N_s+2}p_{20} + \cdots + M_{1,M_s(N_s+1)}p_{M_sN_s}$$
$$+ M_{1,M_s(N_s+1)+1}q_{10} + \cdots + M_{1,(1+M_s)(N_s+1)}q_{1N_s}$$
$$+ M_{1,(1+M_s)(N_s+1)+1}q_{20} + \cdots + M_{1,2M_s(N_s+1)}q_{M_sN_s}\}\,\mathrm{e}^{\mathrm{j}\omega t}. \tag{11}$$

The equations of motion for the free vibration of the cylinder with masses is then given, using Lagrange's equations, as $\mathrm{d}/\mathrm{d}t(\partial T_{tot}/\partial \dot{p}_{m_sn_s}) + \partial U_{cyl}/\partial p_{m_sn_s} = 0$ and $\mathrm{d}/\mathrm{d}t(\partial T_{tot}/\partial \dot{q}_{m_sn_s}) + \partial U_{cyl}/\partial q_{m_sn_s} = 0$, with $T_{tot} = T_{cyl} + T_{m_1} + T_{m_2} + \cdots + T_{m_n}$, in which case

$$\left[[\mathbf{M}] + \sum_k [\mathbf{M}_k]\right]\cdot\begin{bmatrix}\ddot{\mathbf{p}}\\ \ddot{\mathbf{q}}\end{bmatrix} + [\mathbf{K}]\cdot\begin{bmatrix}\mathbf{p}\\ \mathbf{q}\end{bmatrix} = \mathbf{0}, \tag{12}$$

where the introduction of the point masses has resulted in coupled equations in the original modal expansion. Assuming harmonic time dependence, $\exp(\mathrm{j}\omega t)$, for the $p_{m_sn_s}$ and $q_{m_sn_s}$ generalized co-ordinates, the natural frequencies ω_{r_s} and corresponding normal modes $\mathbf{v}_{r_s}^{\mathrm{T}} = \{\mathbf{p}_{r_s}^{\mathrm{T}}\ \mathbf{q}_{r_s}^{\mathrm{T}}\}$ are obtained by solving the characteristic equation given by

$$\det\left([\mathbf{K}] - \omega_{r_s}^2\left[[\mathbf{M}] + \sum_k [\mathbf{m}_k]\right]\right) = 0. \tag{13}$$

The terms ω_{r_s} and $\mathbf{v}_{r_s}$ are called the 'new' natural frequencies and structural modes of the cylinder respectively.

2.3. THE EXTERNAL FORCE ON THE CYLINDER DUE TO THE ACOUSTIC FIELD

The generalized force $F_{r_s}(\omega, \phi_i)$ exciting each structural mode r_s is calculated for the case of an incident plane wave acoustic field at a frequency ω and with wavenumber vector at an incidence angle ϕ_i to the axis of the cylindrical shell, and lying in the plane $(x, \theta_i = 0)$ [23]. The generalized force can be expressed as a sum of products of the scattering coefficients of the acoustic field and an external coupling coefficient for a unit incident pressure amplitude component with specified axial wavenumber and circumferential order.

The scattering coefficient $\sigma_{n_s}(\omega, \phi_i)$ of the circumferential cosine component of order n_s of an acoustic plane wave is [23]

$$\sigma_{n_s}(\omega, \phi_i) = \frac{2}{\pi k_z R_e}\left|\frac{\varepsilon_{n_s} j^{n_s+1}}{\mathrm{H}'_{n_s}(k_z R_e)}\right| = \varepsilon_{n_s}\,\bar{\sigma}_{n_s}(\omega, \phi_i), \tag{14}$$

where $\varepsilon_{n_s} = 1$ if $n_s = 0$, $\varepsilon_{n_s} = 2$ if $n_s \neq 0$, $\bar{\sigma}_{n_s}(\omega, \phi_i) = (2/\pi k_z R_e)|\, j^{n_s+1}/H'_{n_s}(k_z R_e)|$, and $H'_{n_s}(k_z R_e)$ is the first derivative with respect to the argument of the Hankel function of the first kind and nth order. (NB the scattering coefficient $\sigma_{n_s}(\omega, \phi_i)$ is dependent on the acoustic wavenumber, $k = \omega/c$, and the normal wavenumber $k_z = k\sin\phi_i$).

Figure 2 shows a set of nine curves for the scattering coefficients σ_{n_s} with $n_s = 0$–8. These scattering coefficients have been calculated with reference to the uniform cylinder analyzed in section 3 that has external radius $R_e = 1{\cdot}7$ m and length $L = 5{\cdot}6$ m. The external acoustic field consists of a plane wave with angle of incidence $\phi_i = 45^\circ$. The nine plots in Figure 2 suggest that, except for the breathing mode of order $n_s = 0$, the scattering coefficient behaves similar to a "low-pass filter" with a cut-off frequency that increases as the

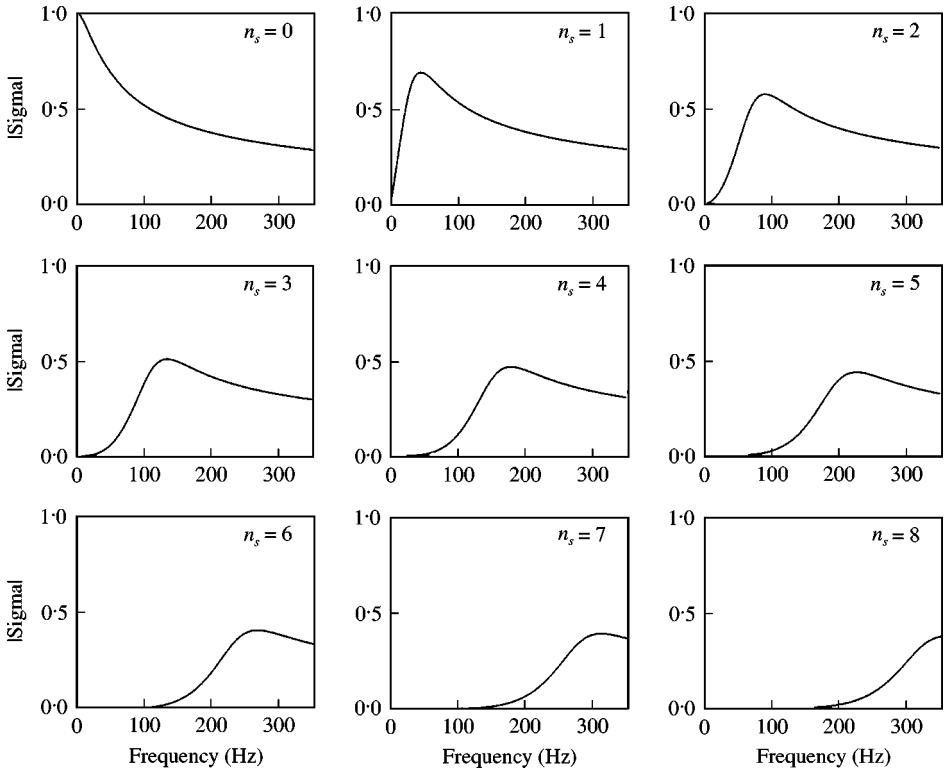

Figure 2. Scattering coefficient as a function of frequency when the acoustic plane wave incidence angle is 45° calculated for different values of n_s.

circumferential modal order n_s rises. The scattering coefficient is characterized by a smooth peak close to the cut-off frequency and its amplitude gradually falls to zero as the frequency tends to infinity.

The nine graphs in Figure 3 show the variation of the scattering coefficients with the incidence angle of the external acoustic field, ϕ_i calculated at a frequency of 200 Hz. The scattering coefficient $\sigma_{n_s}(\omega, \phi_i)$ for $n_s = 0$ varies with a "saddle function" from a maximum of 1 for $\phi_i = 0^\circ$ and 180° (grazing angles) and a minimum of about 0·4 for $\phi_i = 90^\circ$. For higher circumferential modal order n_s the saddle function is restricted to an increasingly smaller angle range $\phi_s \leqslant \phi_i \leqslant (180^\circ - \phi_s)$. For angles outside this band, i.e., for $\phi_i < \phi_s$ and $\phi_i > (180^\circ - \phi_s)$, the scattering coefficient is very low. The circumferential mode order increases as the range becomes smaller and the maximum of the saddle function is also reduced. For high enough values of n_s, for example $n_s = 7, 8, \ldots,$ the saddle function of the scattering coefficient falls off to a smooth peak, as can be seen in the lower graphs in Figure 3.

The excitation of the structural modes has been described by the external coupling coefficient $C^{ext}_{m_s n_s}(\omega, \phi_i)$, for a unit amplitude pressure distribution on the cylinder surface, $\Theta_{m_s n_s}$, that has axial wavenumber $k_x = k\cos\phi_i$ and circumferential order n_s:

$$C^{ext}_{m_s n_s}(\omega, \phi_i) = \frac{1}{S_e}\int_{S_e} \Theta_{m_s n_s}(\mathbf{r}_s, \phi_i)\, \Psi_{m_s n_s}(\mathbf{r}_s)\, \mathrm{d}S_e = \frac{1}{S_e}\int_{S_e} \cos(n_s\theta)\mathrm{e}^{-\mathrm{j}k_x x}\cos(n_s\theta)\sin\left(\frac{m_s\pi x}{L}\right)\mathrm{d}S_e. \tag{15}$$

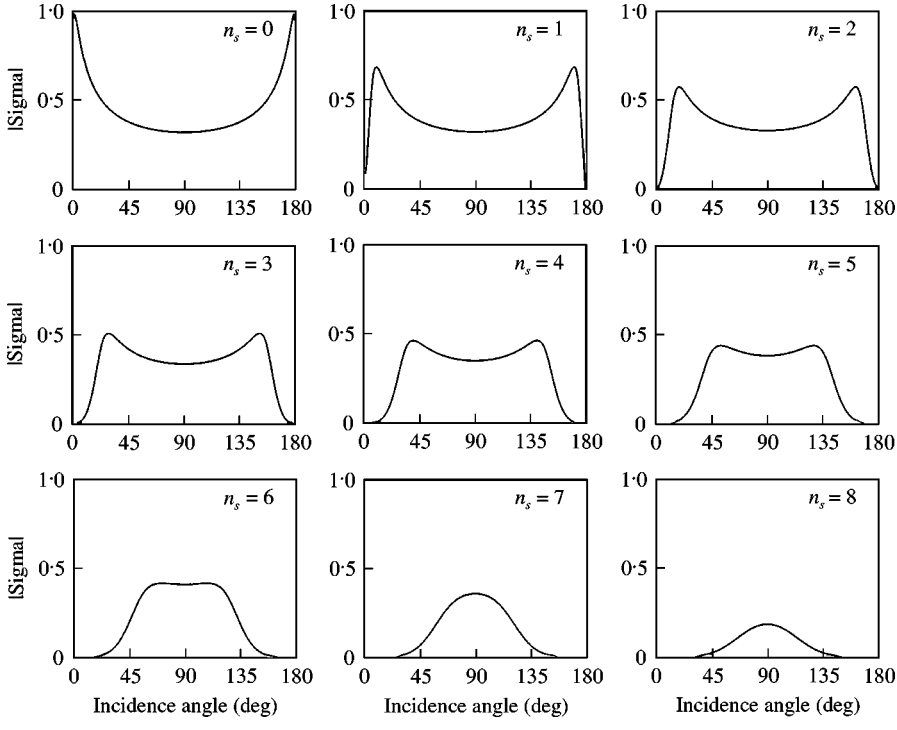

Figure 3. Scattering coefficient as a function of the incidence angle of the acoustic plane wave at a frequency of 200 Hz calculated for different values of n_s.

The external field is assumed symmetric with respect to $\theta_i = 0^\circ$, hence the excitation couples into the cosine components of the structural mode $\Psi_{m_s n_s}$ only. Therefore, the external coupling coefficient $C^{ext}_{m_s n_s}(\omega, \phi_i)$ is given by

$$C^{ext}_{m_s n_s}(\omega, \phi_i) = \frac{m_s \pi}{\alpha_{n_s} L^2} \left[\frac{(-1)^m \, \mathrm{e}^{-\mathrm{j} k_x L} - 1}{k_x^2 - (m_s \pi / L)^2} \right], \tag{16}$$

where if $n_s = 0$ then $\alpha_{n_s} = 1$, otherwise $\alpha_{n_s} = 2$. In the particular case where $k_x = m_s \pi / L$ the asymptotic value of the coupling coefficient $C^{ext}_{m_s n_s}(\omega, \phi_i)$ has been calculated by deriving the indeterminate limit for $k_x \to m_s \pi / L$ with l'Hôpital's rule, so that $C^{ext}_{m_s n_s}(\omega, \phi_i) = -\mathrm{j} 2 \alpha_{n_s}$. Figure 4 shows a set of nine curves for the external coupling coefficients $C^{ext}_{m_s n_s}(\omega, \phi_i)$ with $m_s = 1$–9 and $n_s = 0$. Also, in this case, the dimensions of the cylinder studied in section 3 have been used. The nine curves indicate that the external coupling coefficient behaves as series of "band pass filters". Indeed, the coupling coefficient is characterized by a series of rounded peaks which are symmetric with reference to the vertical axis of the plot and whose amplitude goes from zero at the frequency boundaries of each band filter $f_c \pm \Delta$, to a maximum at the centre frequency of each band filter f_c. The maximum value of these peaks is not constant. The band pass filter has maximum amplitude dependent upon the mode number m_s. For $m_s = 1$, the higher peak is for the band pass filter with centre frequency equal zero, $f_c = 0$ Hz. The frequency for the peak maximum amplitude rises as the mode number n_s rises.

The nine curves in Figure 5 show the variation of the external coupling coefficients with reference to the incidence angle of the external acoustic field ϕ_i calculated at a discrete

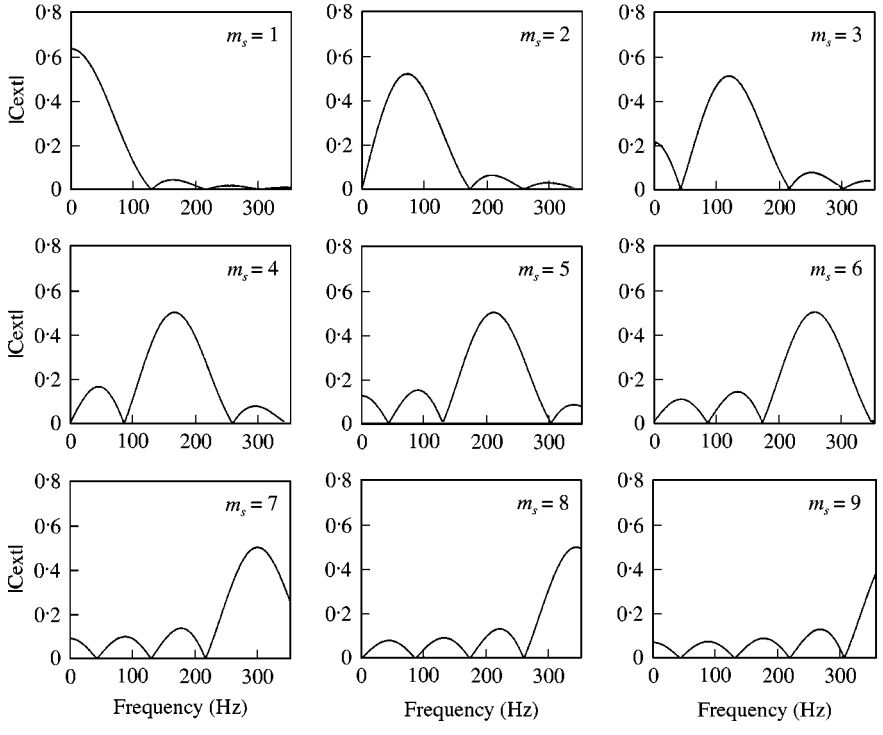

Figure 4. External coupling coefficient as a function of frequency when the acoustic plane wave incidence angle is 45° calculated for different values of m_s.

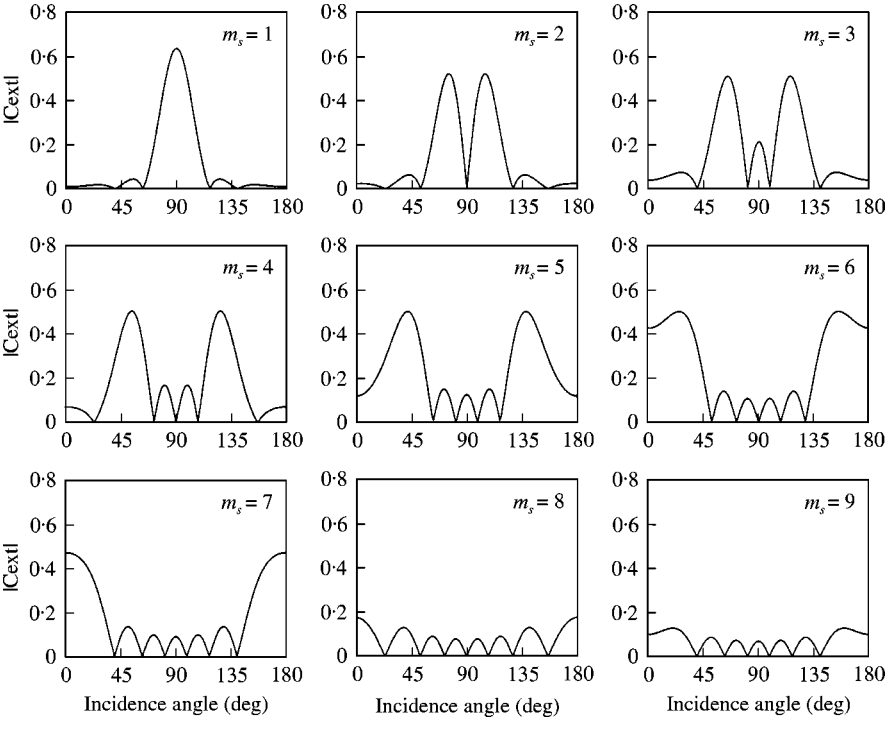

Figure 5. External coupling coefficient as a function of the incidence angle of the acoustic plane wave at a frequency of 200 Hz calculated for different values of m_s.

frequency of 200 Hz. The external coupling coefficient function $C^{ext}_{m_s n_s}(\omega, \phi_i)$ for $m_s = 1$ is characterized by a smooth peak in an angle range $\phi_e \leqslant \phi_i \leqslant (180^\circ - \phi_e)$, where $\phi_e \cong 60^\circ$, with a maximum for $\phi_i = 90^\circ$. Outside the angle band of this "central peak" the external coupling factor is characterized by a series of peaks which, however, are relatively small. As the number of axial mode order m_s rises, the number of smoothed peaks or ripples in the angle band $\phi_e \leqslant \phi_i \leqslant (180^\circ - \phi_e)$ increases. For example, for $m_s = 4$ there are four peaks between $25^\circ \leqslant \phi_i \leqslant 155^\circ$. In general, the peaks with maximum amplitude are those corresponding to the lower and higher angles of incidence. The others tend to have much smaller peak amplitudes. In particular, for $m_s = 7$, the external peaks occur for grazing angles and the central peaks have particularly low amplitude indicating a small coupling effect for angle of incidence close to normal. For higher axial mode orders there are no "external peaks" and a series of relatively small internal peaks are obtained for $\phi_i = 0^\circ - 180^\circ$.

The contribution to the total generalized force $F_{r_s}(\omega, \phi_i)$ in the r_sth mode, due to the m_s and n_s modal orders can be expressed as follows:

$$F_{r_s m_s n_s}(\omega, \phi) = S_e C^{ext}_{m_s n_s}(\omega, \phi_i) p_{r_s m_s n_s} \sigma_{n_s}(\omega, \phi_i), \tag{17}$$

where $p_{r_s m_s n_s}$ is the relative amplitude of the (m_s, n_s) cosine component of the r_sth mode. So the total generalized force in the r_sth mode, summed over all of the components of the external field, is

$$F_{r_s}(\omega, \phi_i) = 2\pi R_e \sum_{n_s=0}^{N_s} \bar{\sigma}_{n_s} \sum_{m_s=1}^{M_s} p_{r_s m_s n_s} \frac{m_s \pi}{L} \left[\frac{(-1)^{m_s} \mathrm{e}^{-\mathrm{j} x_x L} - 1}{k_x^2 - (m_s \pi / L)^2} \right]. \tag{18}$$

According to the limit derived for equation (16), when $k_x = m_s \pi / L$ the total generalized force in the r_sth mode is given by $F_{r_s}(\omega, \phi_i) = 2\pi R_e \sum_{n_s=0}^{N_s} \bar{\sigma}_{n_s} \sum_{m_s=1}^{M_s} p_{r_s m_s n_s} (-\mathrm{j}/2\alpha_{n_s})$. In the specific case of a cylinder without masses each new structural mode exactly corresponds to a cylinder mode of order (m_s, n_s). In this case, the external excitation evaluated for a specific new structural mode r_s, that is, for a specific cylinder mode of order (m_s, n_s), is given by the product of the scattering coefficient σ_{n_s} and the external coupling coefficient $C^{ext}_{m_s n_s}$.

According to the plots shown above, the combination of the scattering and external coupling factors produces a "filtering effect" where at each frequency and at each incidence angle ϕ_i only a limited number of structural modes are actually well coupled to the external acoustic plane wave. Indeed at certain frequencies, and for certain incidence angles ϕ_i, this filtering effect can be so effective that even the few modes coupled to the external acoustic field are actually weakly coupled. The idea explored in this paper of attaching blocking masses on the cylinder in such a way as to modify the structural modes was also aimed at reducing the response of these modes to the external field at certain frequencies.

2.4. CALCULATION OF THE UNCOUPLED SHELL MODAL RESPONSE $T_{r_s m_s n_s}(\omega, \phi)$ *FOR THE* r_s MODE OF THE SHELL THAT HAS AN (m_s, n_s) COMPONENT

For the general case with each mode of the shell expressed as a sum of circumferential and axial orders, the response can be calculated using superposition of the response of the mode due to the forcing in each individual (m_s, n_s) component

$$T_{r_s m_s n_s}(\omega, \phi) = \left[\frac{F_{r_s} p_{r_s m_s n_s} \cos n_s \theta}{\Lambda_{r_s}(\omega_{r_s}^2 - \omega^2 + \mathrm{j}\eta_{m_s n_s} \omega_{r_s} \omega)} + \frac{F_{r_s} q_{r_s m_s n_s} \sin n_s \theta}{\Lambda_{r_s}(\omega_{r_s}^2 - \omega^2 + \mathrm{j}\eta_{m_s n_s} \omega_{r_s} \omega)} \right] \sin \frac{m_s \pi x}{L}, \tag{19}$$

where Λ_{r_s} is the modal mass which is given by

$$\Lambda_{r_s} = \rho_c h \int_S \left[\sum_{m_s=1}^{M_s} \sum_{n_s=0}^{N_s} \left(p_{r_s m_s n_s} \cos n_s\theta \sin\left(\frac{m_s \pi x}{L}\right) + q_{r_s m_s n_s} \sin n_s\theta \sin\left(\frac{m_s \pi x}{L}\right)\right)\right]^2 \mathrm{d}S_i$$

$$= \rho_c h R_i \frac{\pi L}{2} [(p_{r_s 10}^2 + p_{r_s 20}^2 \quad + \cdots + p_{r_s M_s 0}^2) + 1]. \tag{20}$$

Therefore, inserting $\delta_{r_s} = p_{r_s 10}^2 + p_{r_s 20}^2 + \cdots + p_{r_s M_s 0}^2$ and using the normalization of the modes:

$$\Lambda_{r_s} = (1 + \delta_{r_s}) \rho_c h \frac{2\pi R_i L}{4} = (1 + \delta_{r_s}) \frac{M_{cyl}}{4}. \tag{21}$$

$\eta_{m_s n_s}$ is the modal loss factor, including structural and acoustic (radiation) losses, which is given by the following relations that are dependent upon wavenumber matching at a particular frequency [23]:

(1) If $\left(\frac{m_s\pi}{L}\right)^2 + \left(\frac{n_s}{R_i}\right)^2 > \left(\frac{\omega_{m_s n_s}}{c}\right)^2$ and if $\left(\frac{n_s}{R_i}\right)^2 < \left(\frac{\omega_{m_s n_s}}{c}\right)^2$

$$\eta_{m_s n_s} = \frac{64 \rho_a L}{m_s^2 \pi^4 \bar{M}_{cyl}} + \eta_{str} \tag{22}$$

(2) If $\left(\frac{m_s\pi}{L}\right)^2 + \left(\frac{n_s}{R_i}\right)^2 > \left(\frac{\omega_{m_s n_s}}{c}\right)^2$ and if $\left(\frac{n_s}{R_i}\right)^2 > \left(\frac{\omega_{m_s n_s}}{c}\right)^2$, i.e., below coincidence

$$\eta_{m_s n_s} = \eta_{str}. \tag{23}$$

(3) If $\left(\frac{m_s\pi}{L}\right)^2 + \left(\frac{n_s}{R_i}\right)^2 < \left(\frac{\omega_{m_s n_s}}{c}\right)^2$

$$\eta_{m_s n_s} = \frac{\rho_a c}{\omega_{m_s n_s} \bar{M}_{cyl}} + \eta_{str}, \tag{24}$$

where $\bar{M}_{cyl} = M_{cyl}/S_i$ is the mass per unit area of the cylinder with honeycomb wall. It is possible to find the total response in an (m_s, n_s) structural distribution by summing over all the r_s modes, i.e.,

$$T_{m_s n_s}(\omega, \phi) = \left[\sum_{r_s=1}^{R_s} \left(\frac{F_{r_s} p_{r_s m_s n_s} \cos n_s\theta}{\Lambda_{r_s}(\omega_{r_s}^2 - \omega^2 + \mathrm{j}\eta_{m_s n_s}\omega_{r_s}\omega)} + \frac{F_{r_s} q_{r_s m_s n_s} \sin n_s\theta}{\Lambda_{r_s}(\omega_{r_s}^2 - \omega^2 + \mathrm{j}\eta_{m_s n_s}\omega_{r_s}\omega)} \right)\right] \sin \frac{m_s \pi x}{L}. \tag{25}$$

The response in the (m_s, n_s)th component can therefore be written in the form:

$$T_{m_s n_s}(\omega, \phi) = [\alpha_{m_s n_s} \cos n_s\theta + \beta_{m_s n_s} \sin n_s\theta] \sin \frac{m_s \pi x}{L}, \tag{26}$$

where

$$\alpha_{m_s n_s} = \sum_{r_s=1}^{R_s} \frac{F_{r_s}(\omega, \phi_i) p_{r_s m_s n_s}}{\Lambda_{r_s}(\omega_{r_s}^2 - \omega^2 + \mathrm{j}\eta_{m_s n_s}\omega_{r_s}\omega)} \tag{27}$$

with $m_s = 1, 2, \ldots, M$ and $n_s = 0, 1, 2, \ldots, N_s$; and

$$\beta_{m_s n_s} = \sum_{r_s=1}^{R_s} \frac{F_{r_s}(\omega, \phi_i) q_{r_s m_s n_s}}{\Lambda_{r_s}(\omega_{r_s}^2 - \omega^2 + \mathrm{j}\eta_{m_s n_s}\omega_{r_s}\omega)} \tag{28}$$

with $m_s = 1, 2, \ldots, M_s$ and $n_s = 1, 2, \ldots, N_s$. The $\alpha_{m_s n_s}$ and $\beta_{m_s n_s}$ terms are equivalent to the modal generalized co-ordinate in a particular (m_s, n_s) component, equal to the generalized modal force multiplied by the equivalent modal receptance. It is preferable to consider the response in this form as this can be coupled more straightforwardly to the internal acoustic modes, rather than the structural response in terms of new modes and their corresponding amplitudes.

2.5. COUPLING OF STRUCTURAL AND ACOUSTIC MODES

The calculation of the coupling factor $C^{int}_{m_s n_s m_a n_a p_a}$ between the cavity acoustic modes of order (m_a, n_a, p_a) and the shell structural modes of order (m_s, n_s) is given by the integral [23, 24]

$$C^{int}_{m_s n_s m_a n_a p_a} = \frac{1}{S_i} \int_{S_i} \Psi_{m_s n_s}(\mathbf{r}_s) \Phi_{m_a n_a p_a}(\mathbf{r}_s)\, \mathrm{d}S, \tag{29}$$

which, for even circumferential modes (cosine component), gives

$$C^{int}_{m_s n_s m_a n_a p_a} = \frac{1}{S_i} \int_{S_i} \sin\frac{m_s \pi x}{L} \cos n_s\theta \cos\frac{m_a \pi x}{L} \cos n_a\theta\, \mathrm{J}_{n_a}(\lambda_{p_a n_a})\, R_i\, \mathrm{d}\theta\, \mathrm{d}z, \tag{30}$$

where J_{n_a} is the Bessel function of first kind of order n_a and the coefficients $\lambda_{p_a n_a}$ can be found in reference [26]. For odd circumferential modes (sine component) equation (30) becomes

$$C^{int}_{m_s n_s m_a n_a p_a} = \frac{1}{S_i} \int_{S_i} \sin\frac{m_s \pi x}{L} \sin n_s\theta \cos\frac{m_a \pi x}{L} \sin n_a\theta\, \mathrm{J}_{n_a}(\lambda_{p_a n_a})\, R_i\, \mathrm{d}\theta\, \mathrm{d}z \tag{31}$$

with $n_s = 0, 1, \ldots, N_s$; $n_a = 0, 1, \ldots, N_a$; $m_s = 1, 2, \ldots, M_s$ and $m_a = 0, 1, \ldots, M_a$. Once the integrals into equations (30) and (31) are calculated, the sine and cosine components can be expressed as follows:

$$C^{int}_{m_s n_s m_a n_a p_a} = \begin{Bmatrix} (1/\pi)_{n=0} \\ (1/2\pi)_{n\neq 0} \end{Bmatrix} \frac{m_s}{m_a^2 - m_s^2} [(-1)^{m_a + m_s} - 1]\, \mathrm{J}_{n_a}(\lambda_{p_a n_a}) \tag{32}$$

with $n_s = n_a = 0, 1, 2, \ldots, N$ and

$$C^{int}_{m_s n_s = n_a m_a n_a p_a} = \left(\frac{1}{2\pi}\right) \frac{m_s}{m_a^2 - m_s^2} [(-1)^{m_a + m_s} - 1]\, \mathrm{J}_{n_a}(\lambda_{p_a n_a}) \tag{33}$$

with $n_s = n_a = 1, 2, \ldots, N$. The terms are equivalent except for the breathing modes of the shell $n_s = 0$, that only exist for the cosine component. If $m_s = m_a, m_a \pm 2, m_a \pm 4, \ldots$ then $C^{int}_{m_s m_a n_a p_a} = 0$

Table 1 shows the values assumed by the coupling coefficient C^{int} assuming $\mathrm{J}_{n_a}(\lambda_{p_a n_a}) = 1$. This Table shows that for each acoustic mode m_a the largest coupling term is given by the two structural modes where $m_s = m_a + 1$ and $m_a - 1$. In general, for any acoustic mode m_a the coupling coefficient is positive if $m_s > m_a$ and it is negative if $m_s < m_a$. The largest

TABLE 1

Internal coupling coefficient C^{int} assuming $J_{na}(\lambda_{na,pa}) = 1$

m_s	$m_a = 0$	$m_a = 1$	$m_a = 2$	$m_a = 3$	$m_a = 4$	$m_a = 5$	$m_a = 6$	$m_a = 7$	$m_a = 8$	$m_a = 9$
1	0·3183	0	−0·1061	0	−0·0212	0	−0·0091	0	−0·0051	0
2	0	0·2122	0	−0·1273	0	−0·0303	0	−0·0141	0	−0·0083
3	0·1061	0	0·1910	0	−0·1364	0	−0·0354	0	−0·0174	0
4	0	0·0849	0	0·1819	0	−0·1415	0	−0·0386	0	−0·0196
5	0·0637	0	0·0758	0	0·1768	0	−0·1447	0	−0·0408	0
6	0	0·0546	0	0·0707	0	0·1736	0	−0·1469	0	−0·0424
7	0·0455	0	0·0495	0	0·0675	0	0·1714	0	−0·1485	0
8	0	0·0404	0	0·0463	0	0·0653	0	0·1698	0	−0·1498
9	0·0354	0	0·0372	0	0·0441	0	0·0637	0	0·1685	0
10	0	0·0322	0	0·0350	0	0·0424	0	0·0624	0	0·1675

coupling coefficients, given by $m_s = m_a \pm 1$, converge, respectively, to $\pm 1/2\pi$ as the acoustic mode order m_a tends to infinity.

2.6. CALCULATION OF THE ACOUSTIC RESPONSE OF THE CAVITY AS SOUND PRESSURE

The steady state harmonic response in the acoustic cavity mode $\Phi_{m_a n_a p_a}$ can be written in the following way:

$$p_{m_a n_a p_a}(r, \theta, x, \omega) = \frac{\rho_a c^2 S_i}{\Lambda_{m_a n_a p_a}} \frac{\Phi_{m_a n_a p_a}}{[\omega^2_{m_a n_a p_a} - \omega^2 + \mathrm{j}\omega\omega_{m_a n_a p_a}\eta_{m_a n_a p_a}]} F_{m_a n_a p_a}, \tag{34}$$

where $F_{m_a n_a p_a}$ is the forcing term relative to the (m_a, n_a, p_a) acoustic cavity mode and the natural frequencies $\omega_{m_a n_a p_a}$ and acoustic modes $\Phi_{m_a n_a p_a}$ are given in Appendix A. The modal mass $\Lambda_{m_a n_a p_a}$ is given by

$$\Lambda_{m_a n_a p_a} = \rho_a \int_V \Phi^2_{m_a n_a p_a}(r, \theta, x)\,\mathrm{d}V, \tag{35}$$

where the integral is calculated in Appendix A. The acoustic mode loss factor $\eta_{m_a n_a p_a}$ can be derived from the quality factor Q giving the ratio of the energy stored divided by the energy dissipated per cycle so that [27]:

$$\eta_{m_a n_a p_a} = \frac{1}{Q} = \frac{\Delta\omega_{m_a n_a p_a}}{\omega_{m_a n_a p_a}}, \tag{36}$$

where $\Delta\omega_{m_a n_a p_a}$ is the frequency bandwidth relative to the mode (m_a, n_a, p_a). The frequency bandwidth can be derived from the decay time using the following formula [27]:

$$\Delta\omega_{m_a n_a p_a} = \frac{2{\cdot}2}{\pi T_{60}}, \tag{37}$$

where T_{60} is the reverberation time which represents the time required for the sound energy density level to decay by 60 dB from its initial value. The reverberation time is given by the following expression [27]:

$$T_{60} = \frac{55{\cdot}25 V_{cav}}{cA}, \tag{38}$$

where A is the absorption, $V_{cav} = \pi R_i^2 L$ is the volume of the cylindrical cavity and c is the speed of sound of the fluid in the cavity. Using equations (36)–(38) and assuming the fluid in the cavity to be air at 20°C, the expression for the acoustic mode loss factor $\eta_{m_a n_a p_a}$ is found to be

$$\eta_{m_a n_a p_a} = \frac{86{\cdot}4cA}{V_{cav}\omega_{m_a n_a p_a}}. \tag{39}$$

The results presented in Section 3 have been derived assuming that the absorption of the cylinder wall is given by $A = 0{\cdot}5\ \mathrm{m}^2$ and assuming the fluid in the cavity to be air at 20°C so that the speed of sound is given by $c = 343$ m/s.

The forcing term, in equation (34), is given by the vibration of the cylinder in the (m_s, n_s) component of the same circumferential order of the acoustic normal mode $\Phi_{m_a n_a p_a}$. Therefore, equation (34) reduces to

$$p_{m_a n_a p_a}(r, \theta, x, \omega) = \frac{\rho_a c^2 S_i \omega^2}{\Lambda_{m_a n_a p_a}} \frac{\cos(m_a \pi x/L)\, \mathrm{J}_{n_a}(\lambda_{p_a n_a} R/R_i)}{[\omega_{m_a n_a p_a}^2 - \omega^2 + \mathrm{j}\omega\omega_{m_a n_a p_a}\eta_{m_a n_a p_a}]}$$

$$\times \sum_{m_s=0}^{M_s} \sum_{r_s=1}^{R_s} (\alpha_{r_s m_s n_s} \cos n_a\theta + \beta_{r_s m_s n_s} \sin n_a\theta) C^{int}_{m_s n_s m_a n_a p_a}\, \mathrm{e}^{\mathrm{j}\omega t} \tag{40}$$

with $n_s = n_a$. Note that this is the response of the pressure field with (m_a, n_a, p_a) order. The total pressure is summed over all cavity modes, i.e., the summation $\sum_{m_a=0}^{M_a} \sum_{n_a=0}^{N_a} \sum_{p_a=0}^{P_a}$ is introduced. Then the pressure at a point in the cavity can be written in the following way:

$$p(r, \theta, x, \omega) = \omega^2 \rho_a c^2 S_i \sum_{m_a=0}^{M_a} \sum_{n_a=0}^{N_a} \sum_{p_a=0}^{P_a} \left[\frac{\cos(m_a \pi x/L)\, \mathrm{J}_{n_a}(\lambda_{p_a n_a} R/R_i)}{\Lambda_{m_a n_a p_a}[\omega_{m_a n_a p_a}^2 - \omega^2 + \mathrm{j}\omega\omega_{m_a n_a p_a}\eta_{m_a n_a p_a}]} \right.$$

$$\left. \times \sum_{m_s=0}^{M_s} (\alpha_{m_s n_s = n_a} \cos n_a\theta + \beta_{m_s n_s = n_a} \sin n_a\theta) C^{int}_{m_s n_s = n_a m_a n_a p_a} \right] \mathrm{e}^{\mathrm{j}\omega t}. \tag{41}$$

N.B. $\sum_{m_s=1}^{M_s} (\alpha_{m_s n_s = n_a} \cos n_a\theta + \beta_{m_s n_s = n_a} \sin n_a\theta)$ is of circumferential order n_a and the summation gives a result of the form [amplitude] $\cos n_a(\theta - \varepsilon)$, where ε is the orientation of the structural response in the n_a order. For a uniform shell one would expect the structural response to be orientated circumferentially to match the direction of the incident acoustic field. Therefore, by altering the structure there is a possibility of minimizing the spatial coupling.

3. CALCULATED NOISE REDUCTION

To assess the effect of mass addition and angle of plane wave incidence, it is appropriate to evaluate the spatial and temporal mean square pressure in the cavity and the noise reduction provided by the structure. The temporal mean square pressure in the cylindrical cavity when the external excitation is harmonic is given by the relation

$$\langle p^2(\mathbf{r}, t)\rangle_t = \tfrac{1}{2}|p(\mathbf{r}, \omega)|^2 = \tfrac{1}{2} p^*(\mathbf{r}, \omega) p(\mathbf{r}, \omega), \tag{42}$$

which, applying the spatial mean square evaluation, becomes

$$\langle p^2(\mathbf{r}, t)\rangle_{Vol,t} = \frac{1}{V}\int_V \tfrac{1}{2}\,|p(\mathbf{r}, \omega)|^2 \mathrm{d}V = \frac{1}{V}\int_0^L \int_0^{2\pi} \int_0^{R_i} \tfrac{1}{2} p^*(\mathbf{r}, \omega) p(\mathbf{r}, \omega) r\, \mathrm{d}r\, \mathrm{d}\theta\, \mathrm{d}x. \tag{43}$$

Using equation (41), the triple integral of equation (43) gives

$$\langle p^2(\mathbf{r}, t)\rangle_{Vol,t} = \frac{(\omega^2\rho_a c^2 S)^2}{2V} \sum_{m_a=0}^{M_a} \sum_{n_a=0}^{N_a} \sum_{p_a=0}^{P_a} \frac{c_1 L(R_i^2/2)\, \mathrm{J}_{n_a-1}(\lambda_{p_a n_a})}{\Lambda^2_{m_a n_a p_a}[(\omega^2_{m_a n_a p_a} - \omega^2)^2 + \omega^2\omega^2_{m_a n_a p_a}\eta^2_{m_a n_a p_a}]}$$

$$\times \pi \left\{ c_2 \left| \sum_{m_s=1}^{M_s} \alpha_{m_s n_s = n_a} C^{int}_{m_s n_s = n_a m_a n_a p_a} \right|^2 + c_3 \left| \sum_{m_s=1}^{M_s} \beta_{m_s n_s = n_a} C^{int}_{m_s n_s = n_a m_a n_a p_a} \right|^2 \right\}, \quad (44)$$

where if $m_a = 0$ then $c_1 = 1$ and if $m_a \neq 0$ then $c_1 = 1/2$. Also, if $n_s = 0$ then $c_2 = 2$ and $c_3 = 0$ and if $n_s \neq 0$ then $c_2 = 1$ and $c_3 = 1$.

The parameter chosen to represent the sound transmission to the cylindrical cavity is the noise reduction NR which is defined as follows, allowing for unit amplitude external incident sound field [24]:

$$NR(\omega) = -10\log_{10}(\langle p^2(\mathbf{r}, t)\rangle_{Vol,t}). \quad (45)$$

The calculations have been performed both at discrete frequencies and for third-octave frequency bands, to allow the influence of modal separation and overlap to be investigated and to give an overall view of the sound reduction effects achieved with blocking masses. The dimensions and physical properties of the cylinder considered have been selected with reference to a 1:5 scale model of the payload fairing section of the ARIANE 5 launcher. Table 2 summarizes the dimensions of the cylinder according to the notation shown in Figure 1. Also, Table 2 details the thickness and physical properties of the two skins and honeycomb core of the sandwich construction. The ring frequency is approximately 208 Hz.

The influence on the noise reduction has been investigated for an acoustic plane wave incident at an angle of $\phi_i = 45^\circ$ to the axis of the cylinder, the results at this angle being indicative of the diffuse field performance [24].

The number of modes that are required in the calculation for the structural response and cavity response has been investigated. Due to the higher structural modal density and the

TABLE 2

Geometry and physical properties of the cylinder with honeycomb wall

Parameter	Value
Internal radius	$R_i = 1{\cdot}7$ m
Length	$L = 5{\cdot}6$ m
Thickness of outer faceplate	$t_1 = 0{\cdot}88$ mm
Thickness of inner faceplate	$t_2 = 0{\cdot}88$ mm
Thickness of core	$t_3 = 24$ mm
Density of outer faceplate	$\rho_1 = 1700$ kg/m^3
Density of inner faceplate	$\rho_2 = 1700$ kg/m^3
Density of core	$\rho_3 = 48{\cdot}7$ kg/m^3
Young's modulus along axial direction (skin)	$E_{1x} = E_{2x} = 66{\cdot}3\times10^9$ N/m^2
Young's modulus along circumferential direction (skin)	$E_{1\theta} = E_{2\theta} = 20{\cdot}4\times10^9$ N/m^2
The Poisson ratio along axial direction (skin)	$\nu_{1x} = \nu_{2x} = 0{\cdot}31$
Shear modulus along axial direction (skin)	$G_{1x} = G_{2x} = 12{\cdot}4\times10^9$ N/m^2
Shear modulus along axial direction (core)	$G_{3x} = 140\times10^6$ N/m^2
Shear modulus along circumferential direction (core)	$G_{3\theta} = 80\times10^6$ N/m^2
Structural loss factor	$\eta_{str} = 0{\cdot}01$

form of the external and internal structural–acoustic couplings, it is important to include many non-resonant structural modes in the calculation of the response, whilst the number of acoustic modes taken into account can be reduced to include only those whose natural frequencies lie within a reasonable bandwidth about the frequency of the excitation being considered. Results are given showing the sensitivity of these approximations.

3.1. SPECTRUM OF THE NOISE REDUCTION FOR THE CYLINDER WITHOUT MASSES

In this section the spectrum of the noise reduction for a cylinder without masses is presented and analyzed. Figure 6 shows the noise reduction in a frequency range 0–353 Hz for the uniform cylinder. According to the formulation for the sound transmission to the cylinder interior described in section 2, there are two main factors that determine the spectrum shown: first, the acoustic excitation of the cylinder (see section 2.3) and second, the weakly coupled response of the cylinder and the air in the interior (sections 2.4–2.7). The effectiveness of the second factor depends on the coupling between the cylinder and internal cavity modes and the response of each structural and acoustic mode which actually decrease as either the acoustic or structural mode is further and further off-resonance.

In Figure 6, the values of the frequencies where relatively low noise reductions are achieved have been marked. Comparing these values with the calculated natural frequencies of the uncoupled interior acoustic cavity (see Table 3) and the natural frequencies for the uncoupled cylinder (see Table 4) it is evident that the majority of the minima are closely related to natural frequencies of the interior cavity as indicated by the $*$ symbols in Table 3. Table 5 lists, in the first column, the eight minima frequencies marked in Figure 6. Columns 2 and 3 list, respectively, the closest cavity natural frequencies to each of the eight resonances and the difference between the minima and acoustic natural frequencies $\Delta f_a = f - f_{m_a n_a p_a}$. Columns 4 and 5 list, respectively, the cylinder natural frequencies that

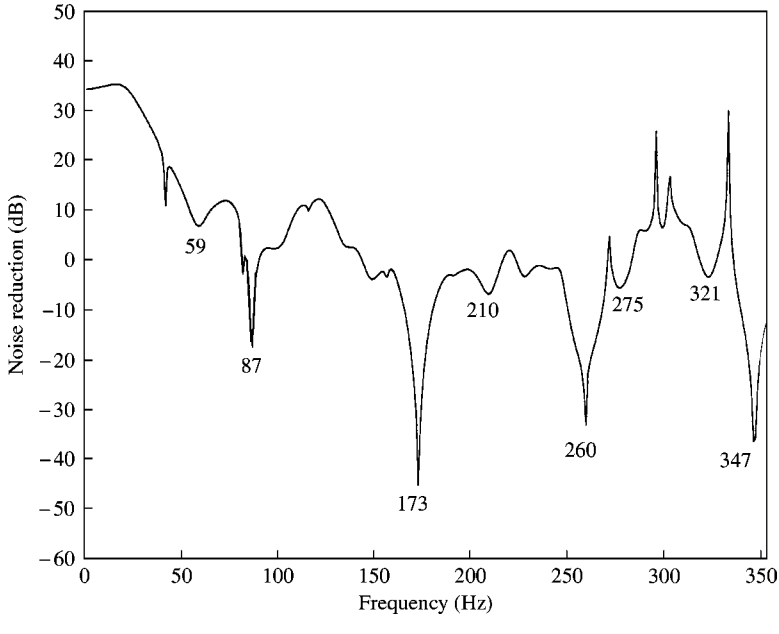

Figure 6. Noise reduction for the honeycomb cylinder without masses excited by a plane acoustic wave of unit amplitude and incidence angle $\phi_i = 45^\circ$.

TABLE 3

Acoustic natural frequencies of the cylindrical cavity (Hz)

m_a	n_a	p_a	f_a	m_a	n_a	p_a	f_a	m_a	n_a	p_a	f_a	m_a	n_a	p_a	f_a
0	0	0	0	7	0	0	214·3	1	1	2	275·8	9	1	1	324·4
1	0	0	30·6	2	5	0	214·9	6	5	0	276·0	2	2	2	325·9
0	1	0	59·0*	0	2	1	215·3	1	7	0	277·1	8	2	1	326·1
2	0	0	61·2	1	2	1	217·5	8	3	0	279·6	0	0	3	326·6
1	1	0	66·5	6	0	1	221·1	2	1	2	280·8	1	0	3	328·1
2	1	0	85·0*	7	1	0	222·3	9	1	0	281·8	6	1	2	330·0
3	0	0	91·8	2	2	1	223·8	2	7	0	282·1	10	0	1	330·0
0	2	0	98·0	0	0	2	225·2	6	2	1	283·0	6	7	0	331·1
1	2	0	102·7	3	5	0	225·5	4	3	1	285·0	2	0	3	332·3
3	1	0	109·2	1	0	2	227·3	5	6	0	285·4	8	0	2	332·8
2	2	0	115·6	6	3	0	227·9	3	1	2	289·1	3	2	2	333·0
4	0	0	122·5	5	4	0	229·3	3	7	0	290·3	4	8	0	333·1
0	0	1	123·0	5	1	1	229·6	6	0	2	290·7	10	3	0	334·6
1	0	1	126·7	2	0	2	233·4	9	2	0	292·5	7	3	1	334·9
3	2	0	134·3	3	2	1	234·1	7	5	0	297·3	5	4	1	335·1
0	3	0	134·9	7	2	0	235·7	0	4	1	298·1	11	0	0	336·8
4	1	0	135·9	4	5	0	239·6	8	4	0	298·6	0	5	1	337·9
2	0	1	137·4	0	6	0	240·8	8	1	1	298·8	1	5	1	339·3
1	3	0	138·3	1	6	0	242·8	5	3	1	299·5	3	0	3	339·3
2	3	0	148·1	3	0	2	243·2	1	4	1	299·7	11	1	0	342·0
5	0	0	153·1	8	0	0	245·0	4	1	2	300·2	4	2	2	342·7
3	0	1	153·5	7	0	1	247·1	4	7	0	301·4	2	5	1	343·4
4	2	0	156·9	4	2	1	247·7	9	0	1	301·8	8	6	0	343·5
3	3	0	163·2	2	6	0	248·5	6	6	0	302·9	0	9	0	343·9
5	1	0	164·1	6	4	0	250·8	7	2	1	303·8	9	5	0	344·1
0	4	0	170·7	6	1	1	251·1	2	4	1	304·3	1	9	0	345·3
0	1	1	171·2	8	1	0	252·0	10	0	0	306·2	5	8	0	345·5
1	4	0	173·4*	7	3	0	253·2	9	3	0	306·8	7	1	2	347·9*
4	0	1	173·6	4	0	2	256·4	0	8	0	309·7	4	0	3	348·9
1	1	1	173·9	5	5	0	256·6	7	0	2	310·9	7	7	0	349·0
2	4	0	181·4	0	3	1	257·4	1	8	0	311·3	2	9	0	349·3
2	1	1	181·8	3	6	0	257·8	10	1	0	311·8	9	2	1	349·7

TABLE 3
continued

m_a	n_a	p_a	f_a	m_a	n_a	p_a	f_a	m_a	n_a	p_a	f_a	m_a	n_a	p_a	f_a
5	2	0	181·8	1	3	1	259·2*	3	4	1	311·9	6	4	1	350·2
4	3	0	182·2	8	2	0	263·8	5	1	2	313·9	3	5	1	350·2
6	0	0	183·7	5	2	1	264·2	5	7	0	315·1	10	4	0	350·6
6	1	0	193·0	2	3	1	264·5	2	8	0	315·7	10	1	1	350·8
3	4	0	193·9	4	6	0	270·2	6	3	1	316·2	11	2	0	350·8
3	1	1	194·2	5	0	2	272·3	8	5	0	320·1	5	2	2	354·8
5	0	1	196·4	3	3	1	273·3	0	2	2	320·1	8	3	1	355·3
5	3	0	204·0	7	4	0	274·0	10	2	0	321·5	9	0	2	355·9
0	5	0	206·0	0	1	2	274·1	1	2	2	321·5	3	9	0	356·0
1	5	0	208·2	8	0	1	274·1	4	4	1	322·3	11	0	1	358·6
6	2	0	208·2	7	1	1	274·3	7	6	0	322·4*	4	5	1	359·4
4	4	0	210·1*	0	7	0	275·4*	3	8	0	323·1				
4	1	1	210·5	9	0	0	275·6	9	4	0	324·2				

TABLE 4

Structural natural frequencies of the uniform honeycomb cylinder (Hz)

m_s	n_s	f_s	m_s	n_s	f_s	m_s	n_s	f_s	m_s	n_s	f_s	m_s	n_s	f_s
1	4	39·0	4	5	156·5	6	6	230·7	7	5	272·0	2	13	315·3
1	3	41·7	3	3	157·5	4	10	232·2	4	0	272·2	8	4	315·5
1	5	50·9	4	7	160·9	5	9	232·8	2	12	272·7	8	3	320·6
1	2	66·8	2	9	162·1	2	11	232·8	6	2	273·0	8	7	322·4
1	6	70·3	4	4	171·5*	6	5	233·2	7	7	277·7*	6	11	325·0
2	5	77·1	4	8	177·9	6	7	236·0	7	4	277·8	8	2	326·7
2	4	81·9	3	9	178·4	6	4	242·7	5	0	279·0	3	13	327·8
2	6	86·9	1	10	187·8	3	1	244·4	3	12	285·7	5	12	329·4
1	7	94·4	5	6	191·3	3	11	246·5	6	1	285·8	8	1	331·5*
2	3	104·8	5	5	195·2	6	8	248·9	7	3	287·1	7	10	333·2
2	7	106·3	2	10	195·9	5	2	251·5	7	8	290·3	8	0	333·4
3	5	116·2	4	3	196·9	6	3	257·1*	6	0	290·7	8	8	335·1
3	6	116·9	5	7	196·9	4	1	259·0	5	11	292·9	4	13	345·7
1	8	122·2	3	2	198·3	5	10	260·4	6	10	294·3	8	9	353·2
1	1	124·0*	4	9	202·3	1	12	265·3	7	2	297·4	1	14	353·4
3	7	129·5	5	4	208·2*	1	0	265·6	4	12	304·6	9	4	357·0
3	4	129·6	3	10	210·5	4	11	266·5	7	1	305·5	9	5	357·6
2	8	132·0	5	8	211·2	2	0	267·4	1	13	308·1	9	3	358·9
2	2	147·8	2	1	212·4	6	9	268·6	7	0	308·6	6	12	359·9
3	8	150·8	1	11	225·1	3	0	268·8	7	9	308·9			
4	6	153·1	5	3	228·3	5	1	271·1	8	5	313·2			
1	9	153·4	4	2	228·9	7	6	271·7	8	6	315·2*			

TABLE 5

Best external and internal coupling between acoustic and structural modes at the eight minima marked in Figure 6

Frequency for minimum sound reduction index f(Hz)	Acoustic natural frequency and mode close to the minima $f_{m_a n_a p_a}$ (Hz)	Difference in (Hz) between the minima and acoustic natural frequencies $\Delta f_a = f - f_{m_a n_a p_a}$	Structural natural frequency and mode well coupling to the acoustic mode $f_{m_s m_s}$ (Hz)	Difference in (Hz) between the minima and structural natural frequencies $\Delta f_s = f - f_{m_s m_s}$	Internal coupling coefficient C^{int} for the structural mode (m_s, n_s) of column 4 and the acoustic mode (m_a, n_a, p_a) of column 2	Generalized force $F_{r_s}(\omega, \phi_i)$ calculated for the structural mode of column 4 at the resonance frequency of column 1
$f_1 = 59{\cdot}0$	$f_a(0, 1, 0) = 59{\cdot}0$	$\Delta f_{a1} = 0$	$f_s(1, 1) = 124{\cdot}0$	$\Delta f_{s1} = -204{\cdot}4$	$C_1^{int} = 0{\cdot}1852$	$\lvert F_{r_s \to 1,0} \rvert = 0{\cdot}26$
$f_2 = 87{\cdot}0$	$f_a(2, 1, 0) = 85{\cdot}0$	$\Delta f_{a2} = -2$	$f_s(1, 1) = 124{\cdot}0$	$\Delta f_{s2} = -39{\cdot}0$	$C_2^{int} = -0{\cdot}0617$	$\lvert F_{r_s \to 1,1} \rvert = 0{\cdot}12$
$f_3 = 173$	$f_a(1, 4, 0) = 173{\cdot}0$	$\Delta f_{a3} = -0{\cdot}4$	$f_s(4, 4) = 171{\cdot}5$	$\Delta f_{s3} = -1{\cdot}9$	$C_3^{int} = 0{\cdot}0339$	$\lvert F_{r_s \to 4,4} \rvert = 0{\cdot}23$
$f_4 = 210$	$f_a(4, 4, 0) = 210{\cdot}1$	$\Delta f_{a4} = -0{\cdot}1$	$f_s(1, 0) = 208{\cdot}2$	$\Delta f_{s4} = -1{\cdot}9$	$C_4^{int} = -0{\cdot}0085$	$\lvert F_{r_s \to 1,0} \rvert = 0{\cdot}22$
$f_5 = 260$	$f_a(1, 3, 1) = 259{\cdot}2$	$\Delta f_{a5} = +0{\cdot}8$	$f_s(6, 3) = 257{\cdot}1$	$\Delta f_{s5} = 2{\cdot}1$	$C_5^{int} = -0{\cdot}0159$	$\lvert F_{r_s \to 6,3} \rvert = 0{\cdot}17$
$f_6 = 275$	$f_a(0, 7, 0) = 275{\cdot}4$	$\Delta f_{a6} = -0{\cdot}4$	$f_s(7, 7) = 277{\cdot}7$	$\Delta f_{s6} = -2{\cdot}3$	$C_6^{int} = 0{\cdot}0015$	$\lvert F_{r_s \to 7,7} \rvert = 0{\cdot}14$
$f_7 = 321$	$f_a(7, 6, 0) = 322{\cdot}4$	$\Delta f_{a7} = -2{\cdot}3$	$f_s(8, 6) = 315{\cdot}2$	$\Delta f_{s7} = -6{\cdot}2$	$C_7^{int} = -0{\cdot}0093$	$\lvert F_{r_s \to 8,6} \rvert = 0{\cdot}17$
$f_8 = 347$	$f_a(7, 1, 2) = 347{\cdot}9$	$\Delta f_{a8} = -0{\cdot}9$	$f_s(8, 1) = 331{\cdot}5$	$\Delta f_{s8} = +16{\cdot}4$	$C_8^{int} = 0{\cdot}0464$	$\lvert F_{r_s \to 8,1} \rvert = 0{\cdot}14$

largely contribute to the sound transmission at each of the eight minima, as indicated by the $*$ symbols in Table 4, and the separation between the minima and cylinder natural frequencies; $\Delta f_s = f - f_{m_s n_s}$. These cylinder natural frequencies have been selected by considering the effects of two factors. First, the best trade off between the internal coupling coefficient C^{int} and the lower difference between the minima frequency and the natural frequency of the cylinder Δf_s (column 5). As described in section 2.5 the best interior coupling is given for $m_s = m_a \pm 1$ and decreases for higher odd values. Also, the greater the difference between the minima frequency and the natural frequency of the cylinder, the smaller is the off-resonance response of the cylinder mode selected. The second factor used to select the natural frequencies of the cylinder takes into account the excitation of the external acoustic field on each mode. Column 6 gives the internal coupling coefficient as equation (33) with reference to the cavity acoustic mode order (m_a, n_a, p_a) and cylinder structural mode order (m_s, n_s) of the natural frequencies in columns 2 and 4 respectively. Column 7 shows the generalized force $F_{r_s}(\omega)$ for the new structural modes r_s corresponding exactly to the cylinder structural mode (m_s, n_s) of column 4 (note that this assumption is valid only in the case of a cylinder without masses).

Table 5 suggests that the most effective minima, $f_3 = 173$, $f_5 = 260$ and $f_8 = 347$ Hz are all characterized by a resonant acoustic mode and a resonant structural mode with a relatively high internal coupling, C^{int}, and generalized force, $F_{r_s}(\omega)$. For example, the minimum at $f_3 = 173$ Hz is characterized by the resonant acoustic mode m_a, n_a, $p_a = 1, 4, 0$, with $\Delta f_a = -0{\cdot}4$Hz, and by the resonant structural mode m_s, $n_s = 4, 4$, with $\Delta f_s = -1{\cdot}9$ Hz, that have an internal coupling factor $C_3^{int} = 0{\cdot}0339$, and a generalized force $|F_{r_s \to 4,4}| = 0{\cdot}23$ at resonance frequency. The other minima that have been marked in Figure 6 are not as effective as these three. The minima at $f_1 = 59$ and $f_2 = 87$ Hz are characterized by an acoustic mode and a structural mode with relatively high coupling factor and generalized force. However, the natural frequencies of the structural modes are well off-resonance (in fact, $\Delta f_{s1} = -204{\cdot}4$ and $\Delta f_{s2} = -39{\cdot}0$ Hz) so that the sound transmission to the resonant cavity is not as effective as for the other three resonant frequencies listed above. The minima at $f_4 = 210$, $f_6 = 275$ and $f_7 = 321$ Hz are characterized by acoustic and structural mode pairs with natural frequencies close to the resonance frequency, however, they are not so effective because their internal coupling factors are relatively small (in fact, $C_4^{int} = -0{\cdot}0085$, $C_6^{int} = 0{\cdot}0015$ and $C_7^{int} = -0{\cdot}0093$).

In general, it can be concluded that poor noise reduction occurs at frequencies where the sound transmission is controlled by both a resonant acoustic cavity mode and a resonant cylinder structural mode that are characterized by a good spatial coupling and an efficient coupling with the external acoustic excitation. This type of conclusion has been derived in an empirical manner rather than from a rigorous mathematical analysis, and therefore it should be considered only as a general engineering guideline for the description of the sound transmission mechanisms to the interior of a cylinder acoustic cavity.

Finally, it is important to note that the noise reduction shown in Figure 6 assumes relatively small values that are even negative for frequencies close to the marked resonances. This is because a relatively small value of the absorption coefficient A has been used in the simulation so that in correspondence to frequencies close to the marked resonances the average sound pressure of the air in the cylindrical cavity is higher than that of the external plane wave incident to the cylinder.

3.2. MODAL EFFECT OF BLOCKING MASSES

The positions of the blocking masses attached to the cylinder have been chosen with reference to the main sound transmission factors described in the previous section for the

cylinder without masses, which are the acoustic excitation of the cylinder and the coupled response of the cylinder and the interior cavity.

In section 2.2, it has been shown that the response of the cylinder with blocking masses is characterized by a new set of natural frequencies f_{r_s} and normal modes r_s consisting of a linear combination of the modes of the uniform cylinder. Therefore, an appropriate choice of the positions of the blocking masses can lead to a set of new structural modes r_s which cannot be efficiently excited by the external acoustic field and do not efficiently couple with the cavity modes.

The external acoustic field, considered in this study, is assumed to be a plane wave with wavenumber vector in the plane $(x, \theta_i = 0)$ so that, considering the circumferential modal order n_s, only the symmetric modes of the cylinder, with reference to $\theta = 0^\circ$, are excited. Figure 7 shows the first 48 mode shapes of the uniform cylinder. The odd columns contain the symmetric modes while the even columns show the antisymmetric modes. The symmetric modes have antinodal line, i.e., maximum amplitude, for $\theta = i(\pi/n_s)$ with $i = 0, 1, \ldots, 2n_s - 1$. If, for example, a set of masses is aligned on the cylinder surface along the axial direction $\theta_m = 0^\circ$, a new set of structural modes r_s is obtained that, as shown in Figure 8, consist of the antisymmetric modes of the uniform cylinder and consist of a entirely new set of mode shapes that in most cases have either a nodal line or a relatively small amplitude for $\theta = 0^\circ$. The mode shapes of Figure 8 correspond to the case where 14 masses of equal weight equal to $W_k = 1{\cdot}43$ kg are attached along the axial direction for $\theta_m = 0^\circ$ and for $x_m = L/2 \pm jL/16$ with $j = 1, 2, 3, 4, 5, 6, 7$. The total weight of the 14 masses is 20 kg, i.e., 8% of the cylinder weight which is 250 kg. Figure 8 shows that, except for a few cases, the masses tend to pin the radial displacement of the cylinder along the axial line for $\theta = 0^\circ$ and many of the new cylinder modes are now close to being antisymmetric. The modification of the mode shape in the circumferential direction is determined along the whole length of the cylinder by the uniform distribution of masses along the axial direction. As a consequence of these modifications brought to the cylinder modes, a lower coupling coefficient is obtained between the external acoustic field and the cylinder vibration.

The new cylinder modes, shown in Figure 8, can also influence the effectiveness of the coupling between the cylinder response and the cavity modes. In particular, the uniform distribution of the masses along the length tends to modify the circumferential mode shapes locally so that the coupling with the acoustic modes, having the same circumferential order, is remarkably reduced. It is interesting to note that some of the new structural modes, as for example the modes shown in row/column = 1/1, 1/3, 1/7, 2/5, 2/8, 3/5, 4/3, 5/2, 5/7 and 6/7, have a relatively large portion of the cylinder surface which has very little deformation amplitude. These modes cannot efficiently couple to the acoustic modes of the cavity which are regular cosine or sine modes. Some of these modes have a peculiar form; for example, the modes in row/column = 3/5 and 5/7 have almost no radial displacement along the whole circumference except in the vicinity of the masses where large displacements are shown. In this case the masses are not pinning the radial displacements at the positions where they are attached. On the contrary, they are vibrating with large amplitudes which indicates that they are storing most of the kinetic energy of the modal vibration which is balanced by the strain energy given by the local and relatively large deformation of the cylinder (like a vibration neutralizer).

The positions of the blocking masses on the cylinder discussed in this section have been chosen with reference to the considerations described above and after a certain number of trials where the masses have been attached on a set of configurations chosen intuitively. For example, the effects of masses applied at $\theta_m = 30, 45, 60$ and 90° have been considered. Also different distributions of the blocking masses along the axial direction have been investigated. This process of using intuitive rules, based on the observations of the sound

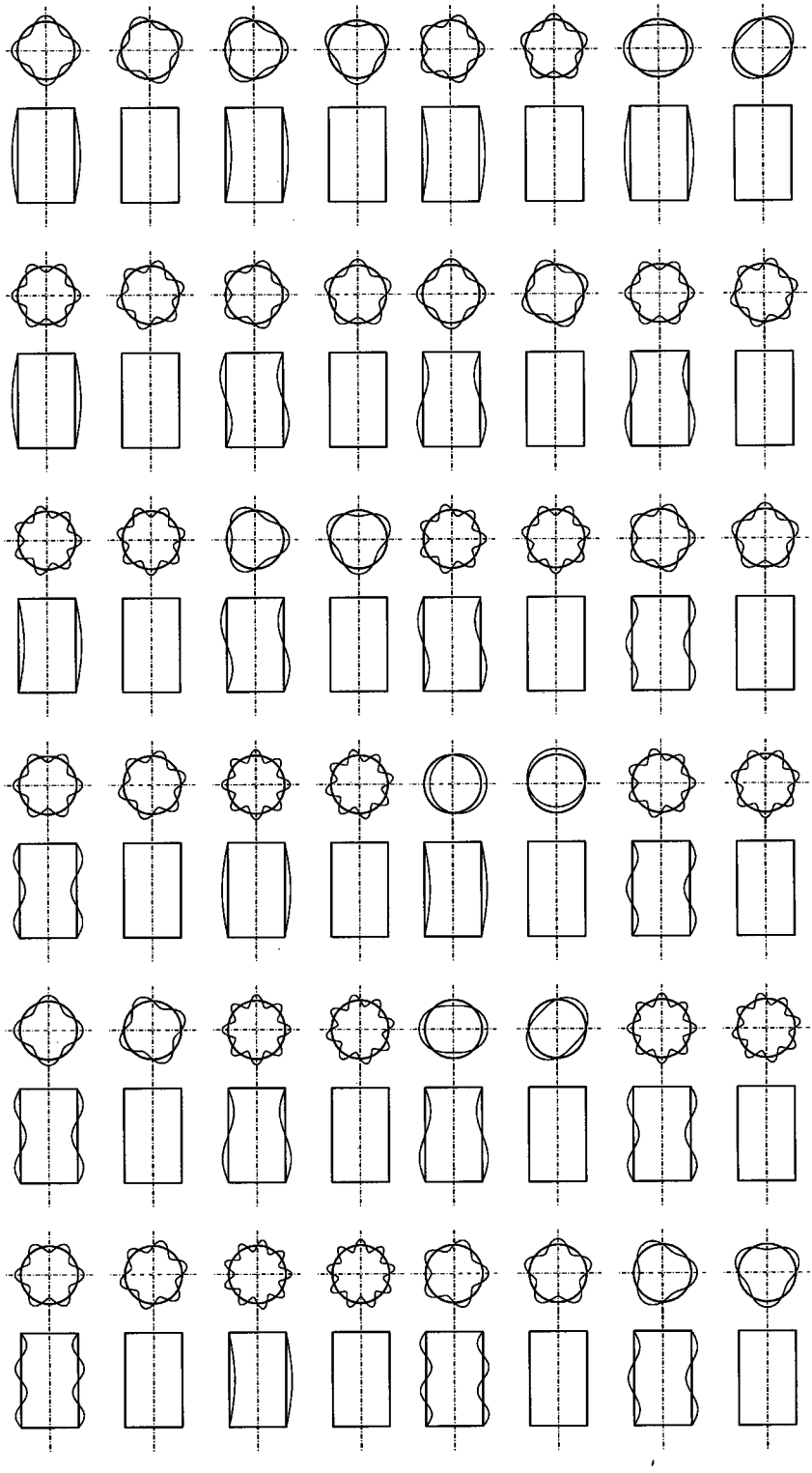

Figure 7. First 48 normal modes of the uniform cylinder.

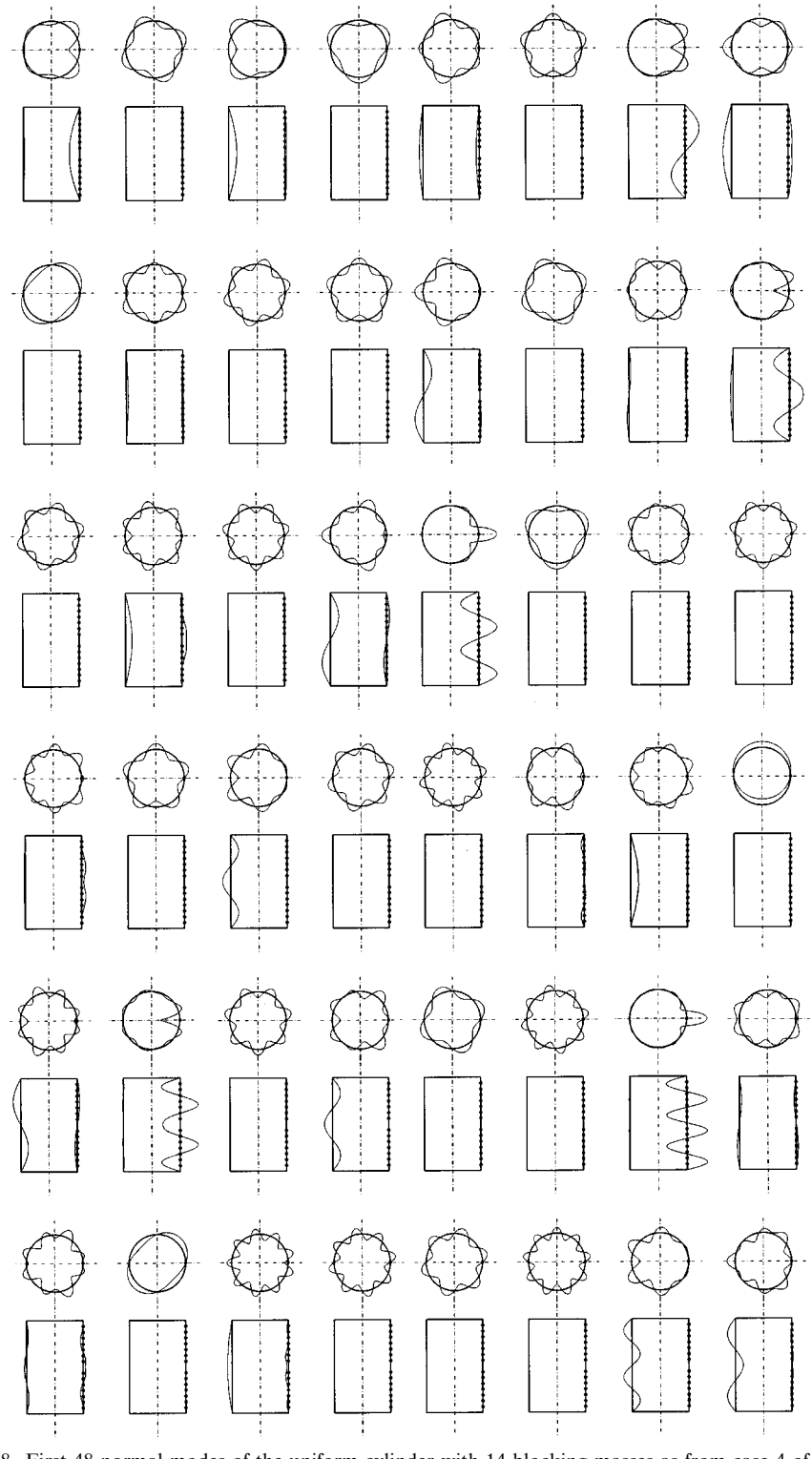

Figure 8. First 48 normal modes of the uniform cylinder with 14 blocking masses as from case 4 of Table 6.

transmission phenomena for the uniform cylinder described previously, and based on the iterative learning process, has led to some conclusions about the ideal position for the blocking masses. However, this study could be improved by developing an optimization approach which would indicate particular geometrical positions for the blocking masses that may give better results than those obtained in this study.

3.3. SPECTRUM OF THE NOISE REDUCTION FOR THE CYLINDER WITH MASSES

The spectrum of the noise reduction for the cylinder with a line of block masses of the same mass, equal to $W_k = 1{\cdot}43$ kg, attached along the axial direction for $\theta_m = 0^\circ$ and for $x_m = L/2 \pm jL/16$ with $j = 1, 2, 3, 4, 5, 6, 7$ is shown in Figure 9. The faint line shows the noise reduction for the cylinder without masses whilst the solid line shows the noise reduction for the cylinder with the attached line of blocking masses. Very little effect is achieved below 180 Hz; indeed, at very low frequency an increase in the sound transmission, rather than a reduction, is shown. However, above 180 Hz the results are very good and reductions of about 10 dB are found.

This type of reduction is very promising but a question which arises is whether this reduction is due to the modifications of the cylinder mode shapes brought about by the blocking masses or is just due to the increased total mass of the cylinder. The answer to this question is given in Figure 10 where the noise reduction for the cylinder with a smeared mass over the surface equal to 20 kg, which is the total of the 14 block masses is shown. From this plot it is evident that, by smearing the equivalent total weight of the block masses over the surface of the cylinder, very little benefit is achieved. Therefore, the reductions shown in Figure 9 are indeed due to the modification of the cylinder mode shapes which produces less efficient excitation of the structure and a less efficient weak-coupling between the structural and acoustic modes.

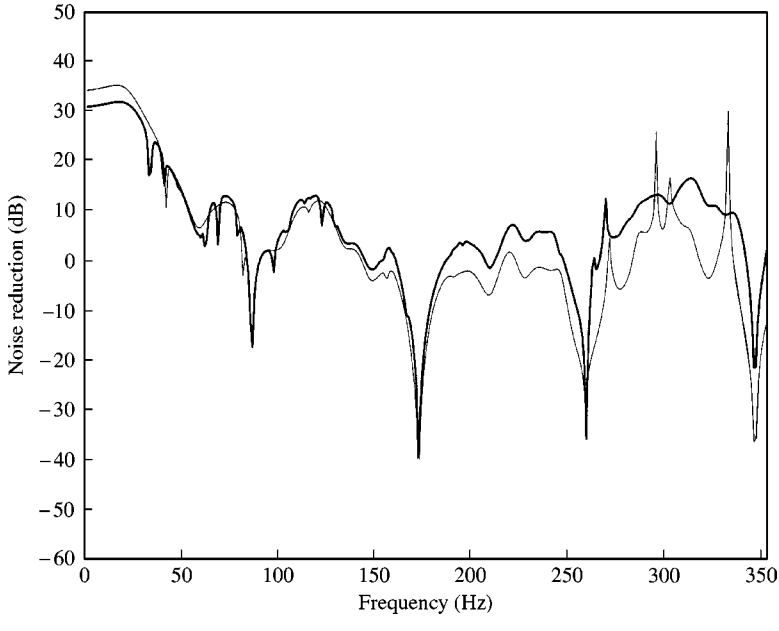

Figure 9. Noise reduction for the honeycomb cylinder with 14 masses (solid line) of 1·4 kg whose positions correspond to case 4 of Table 6 and $\theta_i = 0^\circ$ and without masses (faint line) excited by a plane acoustic wave of unit amplitude and incidence angle $\phi_i = 45^\circ$.

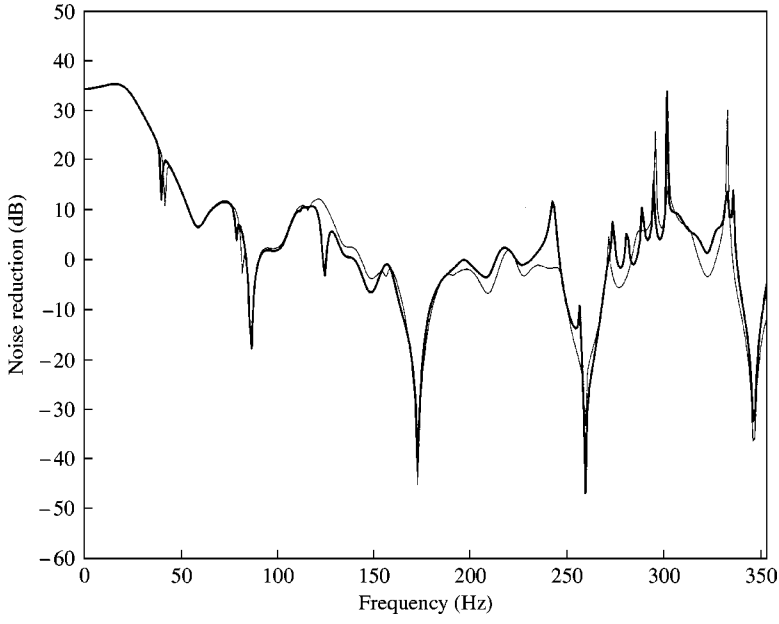

Figure 10. Noise reduction for the honeycomb cylinder with a smeared mass of 20 kg over the cylinder lateral surface (——) and without masses (——) excited by a plane acoustic wave of unit amplitude and incidence angle $\phi_i = 45^\circ$.

3.4. ONE-THIRD OCTAVE FREQUENCY BAND ANALYSIS

In this section the reductions of sound transmission to the cylinder interior due to the blocking masses are summarized in one-third octave frequency bands. Together with the analytical study of sections 3.2 and 3.3, a synthesis study is presented which provides an engineering indication of the type of sound transmission reduction that can be achieved.

The noise reduction for the ith one-third octave frequency band has been calculated using the following relation:

$$NR(\omega_{ci}) = \frac{1}{\omega_{ui} - \omega_{li}} \int_{\omega_{li}}^{\omega_{ui}} NR(\omega)\,\mathrm{d}\omega \approx \frac{1}{\omega_{ui} - \omega_{li}} \sum_{k=1}^{N_i} NR(\omega_k)\Delta\omega_i, \tag{46}$$

where ω_{ci}, ω_{li} and ω_{ui} are, respectively, the centre, lower and upper frequencies of the ith one-third octave frequency band, N_i is the number of frequency samples used for the discretized calculation of the ith one-third octave frequency band noise reduction and $\Delta\omega_i = (\omega_{ui} - \omega_{li})/N_i$.

The excitation considered in this section is still an harmonic plane wave oriented with angles $\theta_i = 0^\circ$ and $\phi_i = 45^\circ$. Therefore, only the line configuration of the block masses has been considered, because of their clear advantage in the reduction of the external coupling between the incident plane wave and the cylinder modal response. Four different distributions of the masses along the axial direction have been considered as described in Table 6. The individual masses considered in each case all have equal weight, chosen in such a way that the total added weight is always 8% of the cylinder weight. A fifth case of a uniform cylinder, with 20 kg mass smeared on its surface, has been used as the benchmark to evaluate the real advantage gained by the blocking masses. The calculation has considered the first 15 one-third octave frequency band containing frequencies up to 703 Hz.

TABLE 6

Positions and mass of the blocking masses

Case No.	No. of masses	Masses (kg)	Angular positions (rad)	Axial position with reference to the cylinder length $x_m = L/2 \pm jL/16$
1	4	5	0	$j = 2, 6$
2	8	2·5	0	$j = 1, 3, 5, 7$
3	12	1·7	0	$j = 1, 2, 3, 5, 6, 7$
4	14	1·4	0	$j = 1, 2, 3, 4, 5, 6, 7$
5	20 kg smeared over the surface of the cylinder			

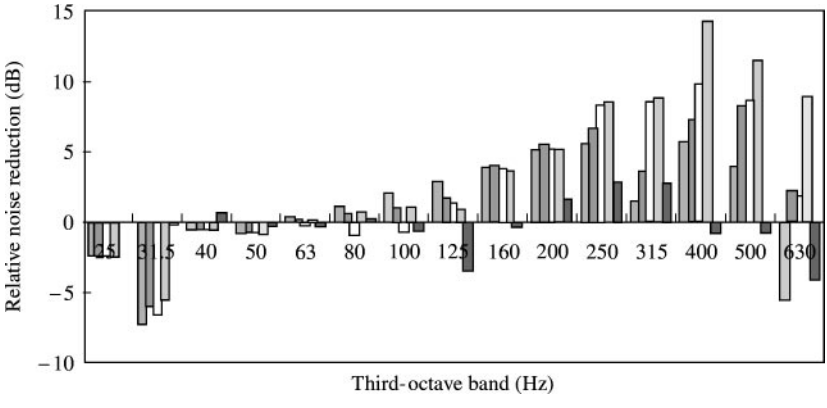

Figure 11. Difference between the noise reduction for the cylinder with additional masses and the cylinder without masses when the cylinder is excited by a plane acoustic wave of unit amplitude and incidence angle $\phi_i = 45°$. ▢, case 1; ▢, case 2; ▢, case 3; ▢, case 4; ▢, case 5.

Figure 11 shows the difference between the noise reduction for the cylinder with the masses (cases 1–4) or with the smeared mass over the cylinder surface (case 5) and the noise reduction for the uniform cylinder. In general, the results obtained indicate that the cases with point masses tend to give greater noise reduction results than the case with a smeared mass over the surface of the cylinder. For all configurations of the masses chosen, good results are obtained for the frequency bands with centre frequency equal and higher than 160 Hz. In contrast for the bands with centre frequency 25 and 31·5 Hz the noise reduction is lower when blocking masses or smeared equivalent mass are used than in the case of a uniform cylinder. In general, the configuration giving best results is that of case number 4.

4. REDUCED ANALYSIS

The calculation of the coupled response of the cylinder and acoustic cavity, with blocking masses attached, requires a relatively large number of summations both over the cylinder modes and the cavity modes as can be deduced from equations (18), (25) and (44). This has meant long computational simulations, particularly to get the noise reduction for the first 15 one-third octave frequency bands. A possible solution to this problem is the reduction of the summations either over the acoustic or the structural modes. For example, the expression of the square sound pressure at a given frequency ω in equation (44) could be reduced by taking into account only the acoustic modes (m_a, n_a, p_a) whose natural

frequencies $\omega_{m_a n_a p_a}$ are within a band of centre frequency ω. This type of reduction of the analysis will be referred to as "*acoustic flagging*". Similarly, the summation of the structural response in the (m_s, n_s)th component, given by equation (25), can be reduced by taking into account only the new structural modes (r_s) whose natural frequencies ω_{r_s} are within a band of centre frequency ω. This type of reduction of the analysis will be referred to as "*structural flagging*". Likewise, the summation over the structural m_s modes into equation (44) can be reduced by taking into account only the modes that are strongly coupled to the acoustic modes. This type of reduction of the analysis will be referred to as "*coupling flagging*".

4.1. "ACOUSTIC FLAGGING"

The selection of the acoustic modes for the reduced analysis has been done with reference to frequency–response considerations. From the plot of Figure 6 it is evident that the noise reduction is characterized by a set of resonances which are determined by the "dominant" acoustic modes. The acoustic modes are well separated and at each frequency the sound pressure in the cavity is determined by a "dominant" mode whose contribution is much higher than that of the "residual" modes. The parameter normally used to identify the prevalence of the response due to a "dominant" mode compared to that of the "residual" modes is the *modal overlap* $M(\omega)$ [28]

$$M(\omega) = \Delta\omega n(\omega), \tag{47}$$

where $\Delta\omega$ is the half-power bandwidth of any one mode at a frequency ω, and $n(\omega)$ is the equivalent modal density, i.e., the average number of modes per unit angular frequency. Therefore, for low values of the modal overlap, normally for $M(\omega) < 1$, the steady state sound pressure in the cylindrical cavity at a certain frequency ω can be approximated by a set of modes with natural frequencies contained in a frequency band $\omega - \Delta\omega \leqslant \omega_{m_a n_a p_a} \leqslant \omega + \Delta\omega$.

Figure 12 shows a set of four plots where the noise reduction at frequency ω has been calculated for the cylinder with four masses (case 1 of Table 6), taking into account the modes with natural frequencies such that $\omega - \omega_1 \leqslant \omega_{m_a n_a p_a} \leqslant \omega + \omega_1$ where $\omega_1/2\pi = 5$, 10, 20, 40 Hz respectively. Because a fixed frequency range has been taken into account, an additional constraint of a lower number of modes to be accounted for has been added. In this way, at low frequencies, where the modal overlap is very small, the frequency range for the selection of the modes is enlarged and enough modes are accounted for the response. In the four plots shown in Figure 12 the lower number of modes to be taken into account for the response has been fixed at 6.

The simulations carried out indicate that an appropriate choice of the frequency range for the selection of the modes used in the computation of equation (44), and of the lower number of modes to be accounted for at each frequency, gives an accurate prediction of the noise reduction in the whole frequency range 0–353 Hz. In particular, Figure 12 shows that when the modes with natural frequency in a frequency band of $\pm$ 40 Hz of the excitation frequency and at least six acoustic modes are accounted for at each frequency, the calculated sound pressure in the cylinder is almost the same as that calculated with the full formulation at every frequency.

4.2. "STRUCTURAL FLAGGING"

Similar to the acoustic flagging procedure, the structural flagging has been carried out with reference to frequency response considerations. In the 0–353 Hz frequency range the

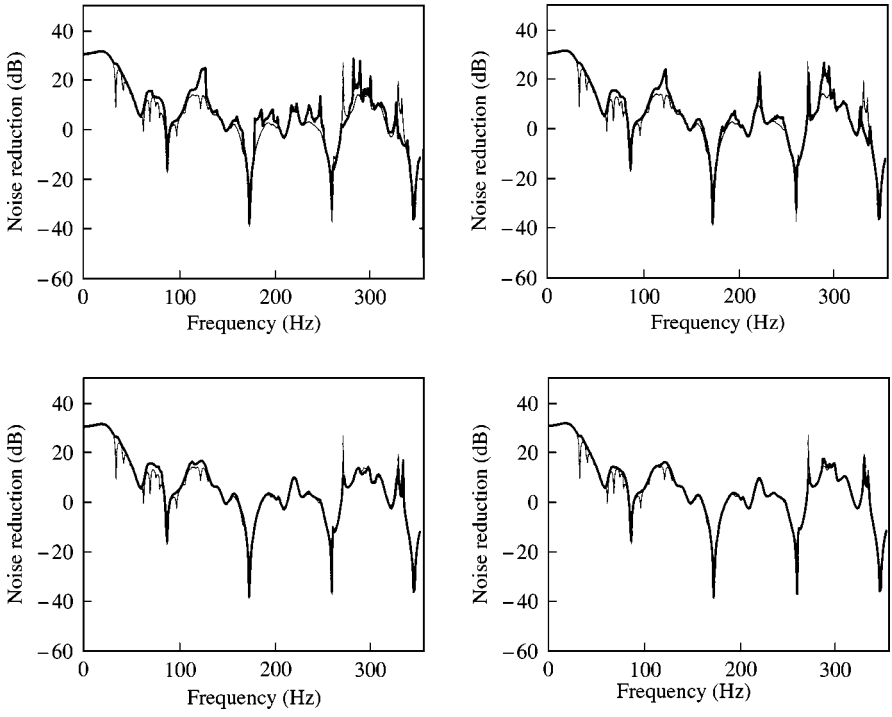

Figure 12. Noise reduction for the honeycomb cylinder with four masses of 5 kg positioned at $x = jL/8$ with $j = 1, 3, 5, 7$ and $\theta_i = 0^\circ$ excited by a plane acoustic wave of unit amplitude and incidence angle $\phi_i = 45^\circ$. ——: complete analysis. ——: reduced analysis that calculates the acoustic pressure in the cylinder cavity at each frequency considering only the acoustic modes with natural frequency within a frequency band of $\pm$ 5 Hz (top left), $\pm$ 10 Hz (top right), $\pm$ 20 Hz (bottom left) and $\pm$ 40 Hz (bottom right). A lower limit for the number of acoustic modes accounted at each frequency is fixed to 6 in the four cases.

cylinder response, equation (25), is characterized by a set of resonances which are determined by the "dominant" new cylinder structural modes. Therefore, also in this case the modal overlap parameter criterion has been used to select the frequency band at each frequency ω that includes the natural frequencies of the new structural modes that mainly contribute to the response of the cylinder. In conclusion, the steady state response of the cylinder at a certain frequency ω given by equation (25) has been approximated by a set of new structural modes r_s with natural frequencies contained in a frequency band $\omega - \omega_1 \leqslant \omega_{r_s} \leqslant \omega + \omega_1$.

Figure 13 shows a set of four plots where the noise reduction at a frequency ω has been calculated for the cylinder with four masses (case 1 of Table 6) taking into account the modes with natural frequencies such that $\omega - \omega_1 \leqslant \omega_{r_s} \leqslant \omega + \omega_1$ where $\omega_1/2\pi = 30$, 40, 50, 60 Hz in the four plots respectively. Also in this case, because a fixed frequency range has been used, an additional constraint of a lower number of 12 new structural modes has been accounted for. In this way, at low frequencies, where the modal overlap is very small, the frequency range for the selection of the modes is enlarged and enough modes are accounted for the response.

The results obtained from the four structural flagging cases considered indicates that the summation over the new structural modes r_s, equation (25), can be limited to a much smaller number of modes without unacceptably reducing the accuracy in the calculation of the noise reduction in the whole frequency range 0–353 Hz. In particular, Figure 13 shows

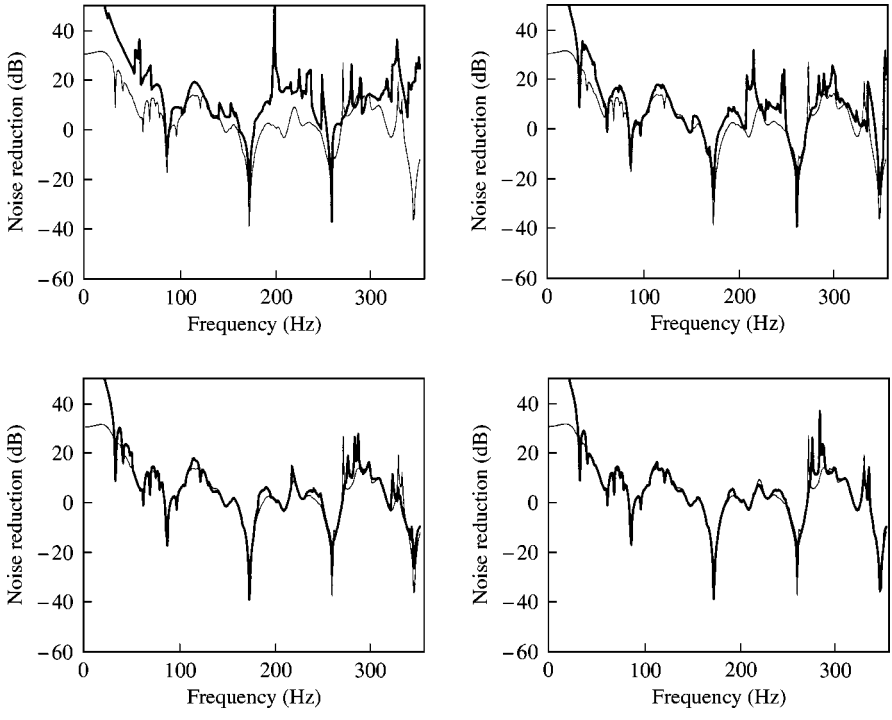

Figure 13. Noise reduction for the honeycomb cylinder with four masses of 5 kg positioned at $x = jL/8$ with $j = 1, 3, 5, 7$ and $\theta_i = 0^\circ$ excited by a plane acoustic wave of unit amplitude and incidence angle $\phi_i = 45^\circ$. ——: complete analysis. ——: reduced analysis that calculates the acoustic pressure in the cylinder cavity at each frequency considering only the cylinder modes with natural frequency within a frequency band of $\pm$ 30 (top left), $\pm$ 40 (top right), $\pm$ 50 (bottom left) and $\pm$ 60 Hz (bottom right). A lower limit for the number of cylinder modes accounted at each frequency is fixed to 12 in the four cases.

that when the new structural modes with natural frequencies in a frequency band of $\pm$ 60 Hz and at least 12 modes are accounted for at each frequency, the calculated cavity sound pressure is quite close to that calculated with the full formulation at every frequency. This is true for all frequencies except those below about 30 Hz. At very low frequency the sound pressure in the cylinder is very low and therefore there is a bigger sensitivity to the "structural flagging".

Comparing the results obtained for the two types of flagging it is evident that the structural flagging requires a larger number of modes at each frequency. This is because the modal overlap factor for the cylinder modes is higher than for the cavity modes.

4.3. "COUPLING FLAGGING"

A final possibility for reducing the number of summations in equation (44) is provided by the summation over the structural m_s modes that can be reduced by taking into account only the modes that are strongly coupled to the acoustic modes. According to section 2.5 the coupling coefficient of structural and acoustic modes is equal to zero $C^{int}_{m_s m_a n_a p_a}(\omega) = 0$ when $m_s = m_a$, $m_a \pm 2$, $m_a \pm 4, \ldots$. Also, the largest coupling coefficient is given by $m_s = m_a \pm 1$ and it progressively reduces for $m_s = m_a \pm \alpha$ with $\alpha = 3, 5, 7, \ldots, \alpha_{max}$.

Figure 14 shows a set of four plots where the noise reduction has been calculated for the cylinder with four masses (case 1 of Table 6) taking into account the structural modes of

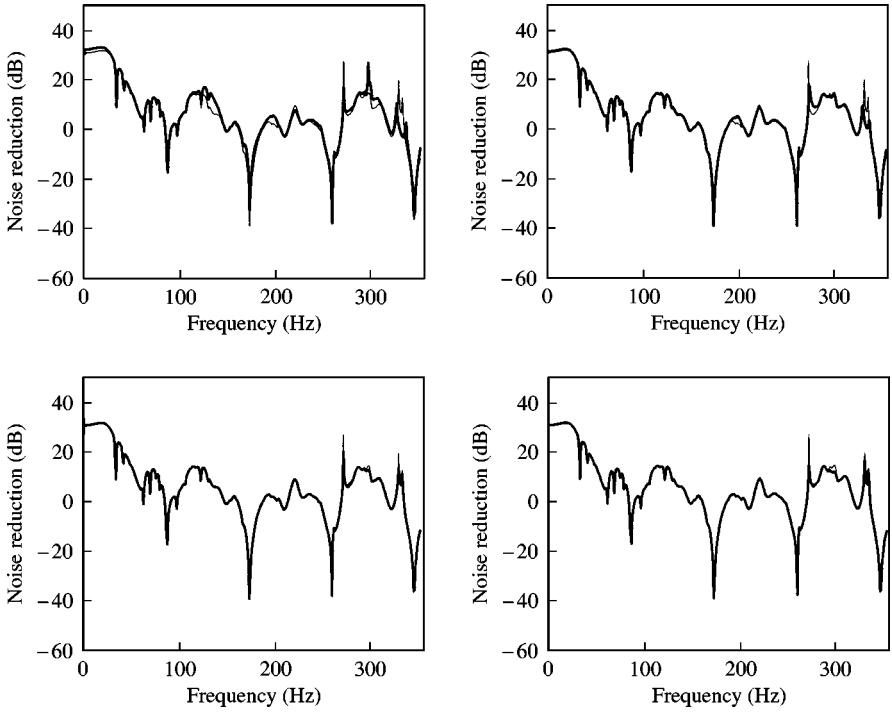

Figure 14. Noise reduction for the honeycomb cylinder with four masses of 5 kg positioned at $x = jL/8$ with $j = 1, 3, 5, 7$ and $\theta_i = 0°$ excited by a plane acoustic wave of unit amplitude and incidence angle $\phi_i = 45°$. ——: complete analysis. ——: reduced analysis that takes into account for the calculation of the acoustic pressure in the cylinder cavity related to each acoustic modes a limited number of structural modes with $m_s = m_a \pm 1$ (top right), $m_s = m_a \pm 1, 3$ (top left), $m_s = m_a \pm 1, 3, 5$ (bottom left) and $m_s = m_a \pm 1, 3, 5, 7$ (bottom right).

order m_s so that $m_s = m_a + 1$, $m_s = m_a \pm 1, 3$, $m_s = m_a \pm 1, 3, 5$ and $m_s = m_a \pm 1, 3, 5, 7$ in the four cases. The n_s mode order is taken to be the same as the circumferential mode order n_a of each acoustic mode taken into account in the summation of equation (44). The results of the simulations suggest that the value of the noise reduction, taking into account the cylinder modes with axial mode order $m_s = m_a \pm 1, 3, 5$, is very accurate. In practice, even by taking into account only the cylinder modes with axial mode order $m_s = m_a \pm 1, 3$, the calculated noise reduction can be considered to be acceptable.

4.4. NOISE REDUCTION USING ACOUSTIC, STRUCTURAL AND MODAL FLAGGING

Having assessed the limits for the frequency range and number of modes required to implement the acoustic, structural and modal flagging a final analysis was performed where the noise reduction was calculated for the cylinder with four masses (case 1 of Table 6). At each frequency the acoustic modes with natural frequency included in the frequency range $\pm$ 40 Hz with a lower limit for the acoustic modes equal to 6, the new structural modes of the cylinder with natural frequency included in the frequency range $\pm$ 60 Hz with a lower limit for the acoustic modes equal to 12, and the cylinder structural modes of indexes $m_s = m_a \pm 1, 3, 5$ are taken into account in the summations of equations (25) and (44).

Figure 15 shows the noise reduction calculated either taking into account all the modes (faint lines) or by implementing simultaneously the acoustic, structural and modal flagging. The result obtained indicates that except at low frequency, there is good agreement between

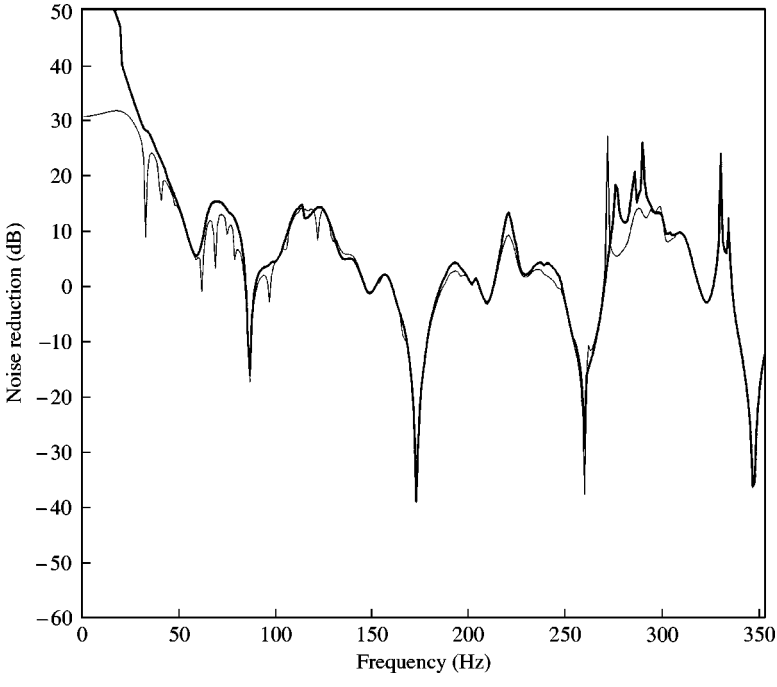

Figure 15. Noise reduction for the honeycomb cylinder with four masses of 5 kg positioned at $x = jL/8$ with $j = 1, 3, 5, 7$ and $\theta_i = 0^\circ$ excited by a plane acoustic wave of unit amplitude and incidence angle $\phi_i = 45^\circ$. ——: complete analysis. ——: reduced analysis that consists of (a) an acoustic reduced analysis that considers at each frequency the modes with natural frequencies in a band of ± 40 Hz with a lower number of modes equal to 6; (b) a structural reduced analysis that considers at each frequency the modes with natural frequencies in a band of ± 70 Hz with a lower number of modes equal to 12 and (c) a mode reduced analysis that considers for each acoustic mode a limited number of structural modes with $m_s = m_a \pm 1, 3, 5$.

the two simulations. This result is even more relevant when one-third octave frequency band analysis is carried out since the noise reduction is averaged over the frequency band so that the small off-resonance mismatching shown in Figure 15 produces very little effect on each value calculated for the one-third octave frequency band noise reduction.

The numerical calculations for the full or reduced models have been performed with the same computer and in the same working conditions. The time required for the reduced analysis has been calculated to be about 3% of the time required for the full analysis. In general, the most effective flagging procedure is the acoustic flagging that most significantly reduces the computational time. Structural flagging still requires a relatively large number of modes and therefore is not as effective as the acoustic flagging. Finally, although the coupling flagging can reduce the last term of equation (44) to few summations, it does not give the same benefits as for the acoustic and structural flagging.

The possibility of reducing the analysis to a few summations over the acoustic and new structural modes at each frequency gives the opportunity of calculating the noise reduction at relatively high frequencies in a relatively short time. However, it must be pointed out that, as the upper limit of frequency analysis rises, the modal overlap factor increases and therefore the modes with natural frequency within a larger frequency band have to be accounted for as the frequency rises. When analysis up to higher frequencies are required it would be ideal to derive an algorithm able to vary the band width for selection of the acoustic and new structural modes at each frequency. This is certainly a more efficient way of reducing the analysis, that should allow the numerical calculations up to several one-third octave frequency bands.

5. CONCLUSIONS

The study presented in this paper has investigated the sound transmission for incident harmonic plane waves to the interior of a honeycomb cylinder filled by air. In particular, the effects of blocking masses placed on the surface of the cylinder has been investigated in order to access the possibility of reducing the external coupling (acoustic plane wave excitation—cylinder response) and internal coupling (cylinder vibration—cavity response) of the system.

For the purposes of this study a modal interaction analysis (MIA) has been developed which is valid in the low-intermediate frequency range and allows the steady state acoustic response of the cavity to be calculated at discrete frequencies for harmonic external plane waves. In this way, the noise reduction at discrete frequencies within one-third octave frequency bands has been evaluated.

The study has considered a set of cases where block masses, with total weight equal to 8% of the cylinder weight, are attached to the cylinder. The simulations carried out show a substantial reduction of the sound transmission in many of the first 15 one-third octave frequency bands. The blocking masses act by modifying the orientation and shape of the cylinder normal modes. In particular, the circumferential re-orientation reduces the coupling mechanism between the incident acoustic field and the cylinder modes. Alternatively, the variation of the structural modes shape, both in the axial and circumferential directions, reduces the coupling between the cylinder modes and the acoustic modes of the interior.

Also, the number of structural and acoustic modes required to predict accurately the sound transmission to the cylinder cavity has been investigated. In particular, the effect of neglecting off-resonance acoustic and structural modes has been considered. It has been shown that in order to have an accurate prediction of the sound transmission it is necessary to take into account the acoustic and structural modes with natural frequencies within an interval of ± 40 and ± 60 Hz of the excitation frequency respectively. Also, the simulations carried out have shown that, in order to represent correctly the coupling effect between the structural and acoustic modes, for each acoustic mode of order (m_a, n_a, p_a) it is necessary to account only for the structural modes with $n_s = n_a$ and $m_s = m_a \pm \alpha$ with $\alpha = 1, 3, 5, \ldots, \alpha_{max}$.

Finally, it has been found that the time required to compute the sound transmission, for a practical example, in a frequency range of 0–353 Hz with the minimum number of acoustic and structural modes required to compute an accurate response at each frequency, can be reduced to 3% of that necessary for the computation of the full response.

ACKNOWLEDGMENTS

Part of the work reported here was supported by the European Space Agency, and in particular the support and collaboration of Mr N. Pinder (ISVR Consultancy Services) is gratefully acknowledged.

REFERENCES

1. L. D. POPE 1970 *Journal of the Acoustical Society of America* **50**, 1004–1018. On the transmission of sound through finite closed shells: statistical energy analysis, modal coupling and nonresonant transmission.

2. S. A. RINEHART and J. T. S. WANG 1972 *Journal of Sound and Vibration* **24**, 151–163. Vibration of simply supported cylindrical shells with longitudinal stiffeners.
3. L. R. KOVAL 1976 *Journal of Sound and Vibration* **48**, 265–275. On sound transmission into a thin cylindrical shell under "flight conditions".
4. M. BARBE, M. GOTTELAND and C. CACCIOLATI 1985 *Revue d'Acoustique* **72**, 77–91. Mécanismes de transfert d'énergie acoustique par une coque cylindrique au voisinage de la fréquence d'anneau.
5. A. BLAISE, M. GOTTELAND, M. BARBE and C. LESUER 1990 *Journal Acoustique* **3**, 361–368. Transmission du son par une coque cylindrique mince isotrope infinie excitée par une onde plane ou un champ diffus.
6. L. R. KOVAL 1979 *Journal of Sound and Vibration* **63**, 51–59. On sound transmission into a orthotropic shell.
7. A. BLAISE, C. LESUEUR, M. GOTTELAND and M. BARBE 1991 *Journal of Sound and Vibration* **150**, 233–243. On sound transmission into an orthotropic infinite shell: comparison with Koval's results and understanding of phenomena.
8. A. BLAISE and C. LESUEUR 1992 *Journal of Sound and Vibration* **155**, 95–109. Acoustic transmission through a 2-D orthotropic multi-layered infinite cylindrical shell.
9. A. BLAISE and C. LESUEUR 1994 *Journal of Sound and Vibration* **171**, 651–664. Acoustic transmission through a "3-D" orthotropic multi-layered infinite cylindrical shell. Part I: formulation of the problem.
10. A. BLAISE and C. LESUEUR 1994 *Journal of Sound and Vibration* **171**, 665–680. Acoustic transmission through a "3-D" orthotropic multi-layered infinite cylindrical shell. Part II: validation and numerical explitation for large structures.
11. L. D. POPE and J. F. WILBY 1977 *Journal of the Acoustical Society of America* **62**, 906–911. Band-limited power flow into enclosures I.
12. L. D. POPE and J. F. WILBY 1980 *Journal of the Acoustical Society of America* **67**, 823–826. Band-limited power flow into enclosures II.
13. L. R. KOVAL 1978 *Journal of Sound and Vibration* **57**, 155–156. On sound transmission into a heavily damped cylinder.
14. L. R. KOVAL 1978 *American Institute of Aeronautics and Astronautics Journal of Aircraft* **15**, 816–821. Effect of longitudinal stringers on sound transmission into a thin cylindrical shell.
15. E. H. DOWELL 1980 *American Institute of Aeronautics and Astronautics Journal of Aircraft* **17**, 690–699. Interior noise studies for single and double walled cylindrical shells.
16. D. A. BOFILIOS and R. VAICAITIS 1987 *American Institute of Aeronautics and Astronautics Journal of Aircraft* **24**, 268–273. Response of double-wall composite shells to random point loads.
17. D. A. BOFILIOS and C. S. LYRINTZIS 1991 *American Institute of Aeronautics and Astronautics Journal* **29**, 1193–1201. Structure-borne noise transmission into cylindrical enclosures of finite extent.
18. L. D. POPE, D. C. RENNISON, C. M. WILLIS and W. H. MAYES 1982 *Journal of Sound and Vibration* **82**, 541–575. Development and validation of preliminary analytical models for aircraft interior noise prediction.
19. L. D. POPE, E. G. WILBY and J. F. WILBY 1987 *Journal of Sound and Vibration* **118**, 449–467. Propeller aircraft interior noise model. Part I: analytical model.
20. J. F. WILBY 1992 *The Shock and Vibration Digest* **24**, 3–13. Noise transmission into propeller driven airplanes II.
21. J. S. MIXON and J. F. WILBY 1995 in *Aeroacoustics of Flight Vehicles. Theory and Practice*, vol. 2, *Noise Control* (H. H. Hubbard, editor) 271–355. Acoustical Society of America, chapter 16. Interior Noise.
22. C. CACCIOLATI, M. GOTTELAND and M. BARBE 1985 *Revue d'Acustique* **72**, 92–101. Transmission d'énergie acoustique par une coque cylindrique finie excitée par des ondes planes externes.
23. J. N. PINDER and F. J. FAHY 1993. *Proceedings of the Institute of Acoustics* **15**, 195–205. A method for assessing noise reduction provided by cylinders.
24. F. J. FAHY 1987 *Sound and Structural Vibration*. London: Academic Press.
25. E. H. BAKER and G. HERRMANN 1966 *American Institute of Aeronautics and Astronautics Journal* **4**, 1063–1070. Vibrations of orthotropic cylindrical sandwich shells under initial stress.
26. L. L. BERANEK and I. L. VÉR 1992 *Noise and Vibration Control Engineering*: *Principles and Applications*. U.S.A.: John Wiley & Sons.
27. D. A. BIES and C. H. HANSEN 1996 *Engineering Noise Control*. London: E & FN Spon.
28. R. H. LYON 1975 *Statistical Energy Analysis of Dynamical Systems*: *Theory and Application*. Boston: MIT Press.

APPENDIX A: NATURAL FREQUENCIES AND NORMAL MODES OF A CYLINDRICAL CAVITY

The acoustic natural frequencies of a cylindrical cavity are derived from the solution of the homogeneous acoustic wave equation in terms of the acoustic pressure p: $\nabla^2 p - \ddot{p}/c^2 = 0$; where $\ddot{p}$ is the second partial derivative with respect to time and ∇^2 is the Laplacian operator with reference to cylindrical co-ordinates x, r, θ. Assuming harmonic time dependence of the form $p = p_0 \exp(\mathrm{j}\omega t)$, the homogeneous Helmoholtz equation $\nabla^2 p_0 + (\omega/c)^2 p_0 = 0$ is obtained which has infinite solutions that could be written in the form $p_{m_a n_a p_a} = \Phi_{m_a n_a p_a}(x, r, \theta) \exp(\mathrm{j}\omega_{m_a n_a p_a} t)$. $\Phi_{m_a n_a p_a}(x, r, \theta)$ are the cavity normal modes and $\omega_{m_a n_a p_a}$ are the correspondent natural circular frequencies in (rad/s). For absorbent walls the normal modes and the natural frequencies are complex. However, for a cylinder with rigid walls and closed ends the normal modes and natural frequencies are real and are given by the following relations [26]:

$$\Phi_{m_a n_a p_a} = \cos\left(\frac{m_a \pi x}{L}\right)\cos(n_a\theta)\, J_{n_a}(\lambda_{p_a n_a} R/R_i) \quad \Phi_{m_a n_a p_a} = \cos\left(\frac{m_a \pi x}{L}\right)\sin(n_a\theta)\, \mathrm{J}_{n_a}(\lambda_{p_a n_a} R/R_i) \tag{A.1, 2}$$

and

$$\omega_{m_a n_a p_a} = c\left(\frac{\lambda^2_{p_a n_a}}{R_i^2} + \frac{m_a^2 \pi^2}{L^2}\right)^{1/2}, \tag{A.3}$$

where the two equations (A.1,2) for the normal modes are required to represent the even and odd circumferential mode shapes. The terms $\lambda_{p_a n_a}$ are given in reference [26] and J_{n_a} is the Bessel function of the first kind and order n_a.

The modes of equations (A.1,2) are normalized such that

$$\int_V \Phi^2(x, r, \theta)\, \mathrm{d}V = \int_0^L \int_0^{2\pi} \int_0^{R_i} \begin{Bmatrix} \cos^2 n_a\theta \\ \sin^2 n_a\theta \end{Bmatrix} \sin^2 \frac{m_a \pi z}{L}\, \mathrm{J}^2_{n_a}(\lambda_{p_a n_a} R/R_i) R\, \mathrm{d}R\, \mathrm{d}\theta\, \mathrm{d}x = \frac{V_{cav}}{\beta}\, \mathrm{J}^2_{n_a - 1}(\lambda_{p_a n_a}) \tag{A.4}$$

and $\beta = 2$ if $n_a = 0$ or $\beta = 4$ if $n_a \neq 0$.

APPENDIX B: NOMENCLATURE

B.1. NOTATION USED FOR THE MODES

$m_s = 1, 2, \ldots, M_s$	axial structural mode number for the cylinder
$n_s = 0, 1, \ldots, N_s$	circumferential structural mode number for the cylinder
$r_s = 1, 2, \ldots, R_s$	structural mode number for the cylinder with block masses
$m_a = 0, 1, \ldots, M_a$	axial acoustic mode number for the cylinder cavity
$n_a = 0, 1, \ldots, N_a$	circumferential acoustic mode number for the cylinder cavity
$p_a = 0, 1, \ldots, P_a$	radial acoustic mode number for the cylinder cavity
u, v, w	in-plane (axial), tangential and flexural (normal to circumference) components of the structural mode

$\Psi_{m_s n_s} = \sin\left(\dfrac{m_s \pi x}{L}\right)\cos(n_s\theta)$

$\Psi_{m_s n_s} = \sin\left(\dfrac{m_s \pi x}{L}\right)\sin(n_s\theta)$

even and odd structural modes

$\Phi_{m_a n_a p_a} = \cos\left(\dfrac{m_a \pi x}{L}\right)\cos(n_a\theta)\,\mathrm{J}_{n_a}(\lambda_{p_a n_a} R/R_i)$

$\Phi_{m_a n_a p_a} = \cos\left(\dfrac{m_a \pi x}{L}\right)\sin(n_a\theta)\,\mathrm{J}_{n_a}(\lambda_{p_a n_a} R/R_i)$

even and odd acoustic modes

$\Theta_{m_s n_s}(\mathbf{r}_s, \phi) = \cos(n_s\theta)\,\mathrm{e}^{-\mathrm{j}k_s x}$ acoustic pressure distribution on the external cylinder surface

$\mathbf{r}_s$ position on the internal surface of the cylinder

H_n Hankel function of the first kind and nth order

J_{n_a} Bessel function of the first kind of order n_a

$p_{m_s n_s}(t),\ q_{m_s n_s}(t)$ generalized co-ordinates of the even and odd structural modes

$A_{m_s n_s}\ B_{m_s n_s}\ C_{m_s n_s}$ relative contributions of the u, v and w displacements in the "new" structural mode

B.2. PHYSICAL PARAMETERS

A absorption

c speed of sound

$\mathrm{d}S = R\,\mathrm{d}\theta\,\mathrm{d}x$ infinitesimal element of the cylinder surface

$h = t_1 + t_2 + t_3$ thickness of the cylinder wall

$k_x = (\omega/c)\cos\phi$ axial wave number

$k_z = (\omega/c)\sin\phi$ normal wave number

L length of the cylinder

$M_{cyl} = (\rho_1 t_1 + \rho_2 t_2 + \rho_3 t_3) S_i$ mass of the cylinder

$\bar{M}_{cyl} = M_{cyl}/S_i$ mass per unit area of the cylinder with honeycomb wall

R_e, R_i external and internal radius of the cylinder

$S_e = 2\pi R_e L$ external surface area of the cylinder

$S_i = 2\pi R_i L$ internal surface area of the cylinder

t_1, t_2, t_3 thickness of the external faceplate, internal faceplate and honeycomb core

$V_{cav} = \pi R_i^2 L$ volume of the cylindrical cavity

$V_{wall} = \pi(R_e^2 - R_i^2)L$ volume of the cylinder wall

ϕ_i angle of incidence of the external acoustic field to the x-axis of the cylinder

$\eta_{m_a n_a p_a}$ modal loss factor for the cavity

$\eta_{m_s n_s}$ modal loss factor for the cylinder vibration (the acoustic damping effect due to the cavity is also taken into account)

η_{str} structural loss factor of the cylinder wall

θ circumferential co-ordinate (in rad)

θ_i angle of incidence of the external acoustic field to the circumferential co-ordinate θ of the cylinder

θ_m circumferential co-ordinate (in rad) of the blocking masses

$\lambda_{p_a n_a}$ coefficient for acoustical modes of a cylinder, from table 6. 2 of reference [26] (these data are stored in a matrix whose row's correspond to values of p_a and whose columns correspond to values of n_a)

$\Lambda_{m_a n_a p_a}$ acoustic modal mass

$\Lambda_{r_s} = 1/4 M_{cyl}$ modal mass for the structural modal summation

ρ_1, ρ_2, ρ_3	density of the external faceplate, internal faceplate and honeycomb core
ρ_a	density of air
$\rho_c = M_{cyl}/V_{wall}$	average density of the cylinder wall
ω	frequency (rad/s)
$\omega_{m_a n_a p_a}$	natural frequency of the (m_a, n_a, p_a)th acoustic mode of a cylindrical cavity with rigid wall (rad/s)
$\omega_{m_s n_s}$	natural frequency of the (m_s, n_s)th structural mode considering a honeycomb cylinder (rad/s)
ω_{r_s}	natural frequency of the r_sth structural mode considering a honeycomb cylinder with applied mass(es) (rad/s)